Available online at www.sciencedirect.com

ScienceDirect

Neuroscience Research 61 (2008) 201–206

Neuroscience Research

www.elsevier.com/locate/neures

# Determination of editors at the novel A-to-I editing positions

Yoshinori Nishimoto [a,b,1], Takenari Yamashita [a,1], Takuto Hideyama [a], Shoji Tsuji [a], Norihiro Suzuki [b], Shin Kwak [a,*]

[a] *Department of Neurology, Graduate School of Medicine, University of Tokyo, 7-3-1 Hongo, Bunkyo-ku, Tokyo 113-8655, Japan*
[b] *Department of Neurology, Graduate School of Medicine, Keio University, 35 Shinanomachi, Shinjuku-ku, Tokyo 160-8582, Japan*

Received 20 December 2007; accepted 29 February 2008
Available online 13 March 2008

**Abstract**

A-to-I RNA editing modifies a variety of biologically important mRNAs, and is specifically catalyzed by either adenosine deaminase acting on RNA type 1 (ADAR1) or type 2 (ADAR2) in mammals including human. Recently several novel A-to-I editing sites were identified in mRNAs abundantly expressed in mammalian organs by means of computational genomic analysis, but which enzyme catalyzes these editing sites has not been determined. Using RNA interference (RNAi) knockdowns, we found that cytoplasmic fragile X mental retardation protein interacting protein 2 (CYFIP2) mRNA had an ADAR2-mediated editing position and bladder cancer associated protein (BLCAP) mRNA had an ADAR1-mediated editing position. In addition, we found that ADAR2 forms a complex with mRNAs with ADAR2-mediated editing positions including GluR2, kv1.1 and CYFIP2 mRNAs, particularly when the editing sites were edited in human cerebellum by means of immunoprecipitation (IP) method. CYFIP2 mRNA was ubiquitously expressed in human tissues with variable extents of K/E site editing. Because ADAR2 underactivity may be a causative molecular change of death of motor neurons in sporadic amyotrophic lateral sclerosis (ALS), this newly identified ADAR2-mediated editing position may become a useful tool for ALS research.


*Keywords:* RNA editing; Adenosine deaminase acting on RNA (ADAR); Immunoprecipitation (IP); RNA interference (RNAi); Cytoplasmic fragile X mental retardation protein interacting protein 2 (CYFIP2); Bladder cancer associated protein (BLCAP)

## 1. Introduction

Adenosine deaminases acting on RNA (ADARs) catalyze A-to-I RNA editing in a wide range of organisms including human. Among three structurally related ADARs (Keegan et al., 2001; Bass, 2002; Maas et al., 2003), ADAR1 is indispensable for normal development (Wang et al., 2000) and ADAR2 plays a key role in the regulation of neuronal excitability in mice (Brusa et al., 1995; Higuchi et al., 2000), and presumably in the pathogenesis of sporadic amyotrophic lateral sclerosis (ALS) in humans, by specifically editing the Q/R site of GluR2, a subunit of the α-amino-3-hydroxy-5-methyl-4-isoxazolepropionic acid (AMPA) receptor (Takuma et al., 1999; Kawahara et al., 2004; Kwak and Kawahara, 2005). Extensive A-to-I conversion occurs in the large numbers of mRNAs (Burns et al., 1997; Higuchi et al., 2000; Wang et al., 2000; Bhalla et al., 2004), and studies using a computational genomic approach have recently demonstrated several novel A-to-I editing sites in mRNAs abundantly expressed in peripheral as well as neuronal tissues (E.Y. Levanon et al., 2005). Using immunoprecipitation (IP) and the RNA interference (RNAi) knockdown system *in vitro*, we investigated whether the recently reported A-to-I editing sites in cytoplasmic fragile X mental retardation protein interacting protein 2 (CYFIP2), filamin A (FLNA), bladder cancer associated protein (BLCAP), and insulin-like growth factor binding protein 7 (IGFBP7) mRNAs (E.Y. Levanon et al., 2005) are the substrates of ADAR1 or ADAR2 in humans. Furthermore, we also investigated whether these mRNAs in humans form complex with ADAR2 by means of ADAR2-immunoprecipitation method on nuclear extracts of human cerebellum.

* Corresponding author.
*E-mail address:* kwak-tky@umin.ac.jp (S. Kwak).
[1] Both these authors equally contributed to this study.

0168-0102/$ – see front matter 
doi:10.1016/j.neures.2008.02.009

## 2. Materials and methods

### 2.1. Isolation of RNA–protein complexes

The nuclear pellet was extracted from 6 g of frozen human cerebella. Briefly, after homogenizing the tissue in ten-volumes of cold 0.25 M sucrose in buffer A (Tris–saline-HCl buffer (pH 7.5) containing 25 mM KCl, 5 mM $MgCl_2$ and 1 mM dithiothreitol), the nuclear pellet was obtained by centrifuging the P1-homogenate in 1.6 M sucrose in buffer A at 130,000 × *g* for 1 h. The RNA–protein complex was isolated from the nuclear pellet according to previously described methods (Ohlson et al., 2005). Briefly, the nuclear pellet was sonicated in 8 ml of ice-cold buffer solution containing 0.1% sodium dodecylsulphate (SDS), 0.5% sodium deoxycholate, 0.5% Igepal CA-630 (Sigma Chemicals, St. Louis, MO) and 1 mM ribonucleoside vanadyl complex (Sigma), and then treated with 800 units of DNase I (Sigma). The resultant solution was centrifuged at 10,000 × *g*, 4 °C for 20 min, and RNA–protein complexes were obtained in the supernatant. All studies were carried out in accordance with the Declaration of Helsinki and the Ethics Committee of the University of Tokyo has approved the experimental procedures used.

### 2.2. Immunoprecipitation of ADAR2-RNA complexes

Stock Sepharose G was prepared by suspending Protein G Sepharose 4 Fast Flow beads (swollen Sepharose G beads; GE healthcare Bioscience, Piscataway, NJ) treated with tRNA (1 mg/ml) and bovine serum albumin (1 mg/ml) in two volumes of phosphate buffered saline (PBS) containing 0.05% of $NaN_3$. First, after pre-clearing once with 50 μl of the untreated Sepharose G suspension in PBS, recombinant ADAR2a and FLAG-ADAR2a proteins which were prepared with TNT T7 Quick for PCR DNA kit (Promega, Madison, WI) were incubated with 50 μl of the stock Sepharose G at 4 °C for 2 h in the presence of 2 μg of either E-20 or C-15 (Santa Cruz Biotechnology, Santa Cruz, CA). Antibody–bead complex was collected by centrifugation and eluted with PBS containing 1% SDS at 65 °C for 10 min. Presence of recombinant ADAR2a and FLAG-ADAR2a proteins in the eluate were verified with western blotting.

Because E-20 more effectively bound to recombinant ADAR2a and Flag-ADAR2a proteins than C-15 (Fig. 1a), we used only E-20 for the immunoprecipitation of nuclear eluate. One ml of the nuclear eluate obtained from 0.75 g of human cerebellum was incubated at 4 °C for 2 h in the presence of 2 μg of E-20 or control goat anti-human IgG (H + L) (Jackson ImmunoResearch, West Grove, PA) after pre-clearing once with 50 μl of the untreated Sepharose G suspension in PBS, and then for another h with additional 50 μl of stock Sepharose G beads. The nuclear eluate–antibody–bead complex was collected by centrifugation and eluted with 50 μl of PBS containing 1% SDS at 65 °C for 10 min and then the eluate was treated with proteinase-K at 37 °C for 60 min. Total RNA was extracted using TRIzol reagent (Invitrogen, Carlsbad, CA).

### 2.3. RNAi of ADAR1 and ADAR2

HeLa cells were cultured in MEMα (Wako, Osaka, Japan), and then in Opti-MEM I Reduced-Serum Medium (GIBCO, Langley, OK) without fetal bovine serum (FBS) or antibiotics, containing 30 nM of one of the small interference RNA (siRNA) listed in Supplementary Table S1 (Qiagen HP GenomeWide siRNAs; Qiagen, Valencia, CA) and Lipofectamine RNAiMAX (1:600; Invitrogen) (Forward Transfection). The following siRNAs were used: siR1a and siR1b were used to target human ADAR1, and siR2a and siR2b to target human ADAR2. Cells cultured in Opti-MEM containing 30 nM ALLStars Negative Control siRNA (siR n/c; Qiagen) were used as the negative control. After 5 h of incubation, the medium was switched back to the original MEMα. Total RNA was extracted 96 h after the administration of siRNAs using an RNA spin Mini RNA Isolation kit (Qiagen), and reverse transcription (RT)-polymerase chain reactions (PCRs) were carried out (Supplementary Tables S1 and S2).

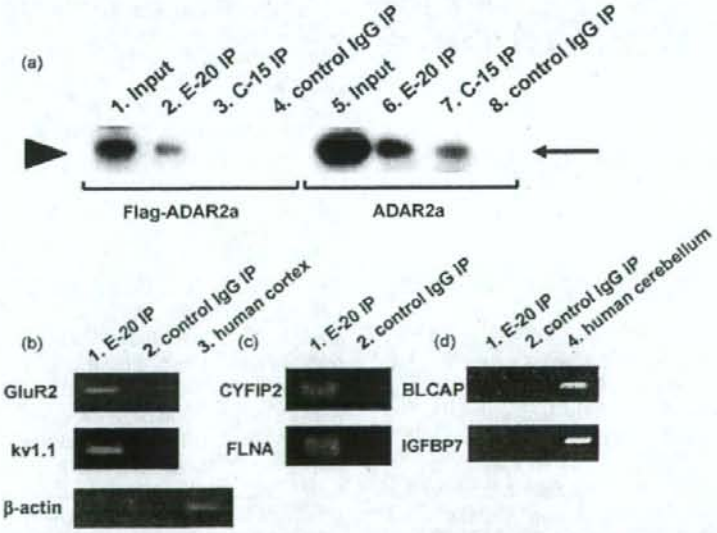


Fig. 1. Immunoprecipitated ADAR2 protein complex specifically contains substrates with selective editing sites. (a) Western blot analysis of eluates immunoprecipitated with anti-human ADAR2 polyclonal antibodies, E-20 (lanes 2 and 6) or C-15 (lanes 3 and 7), containing recombinant Flag-ADAR2a (lanes 2–4) or ADAR2a proteins (lanes 6–8) synthesized *in vitro*. Goat anti-human IgG (H + L) was used as a precipitating control (lanes 4 and 8). Untreated recombinant Flag-ADAR2a (lane 1) and ADAR2a proteins (lane 5) are also shown. Flag-ADAR2a (arrowhead) and ADAR2a proteins (arrow) were immunoprecipitated more effectively by E-20 than by C-15 or control goat anti-human IgG. Total RNA was extracted from the eluate of immunoprecipitate (IP) with E-20 and that of control IgG. (b–d) RT-PCR conducted on these eluates demonstrated mRNAs of GluR2 and kv1.1 (b) (known to have ADAR2-mediated editing sites) as well as those of CYFIP2 (cytoplasmic fragile X mental retardation protein interacting protein 2) and FLNA (filamin A) (c) in the IP with E-20 (lane 1) but not that with control goat anti-human IgG (lane 2). The mRNA of β-actin demonstrated in total RNA extracted from the human cortex (b, lane 3) was not detected in either of the eluates (b). Moreover, both the mRNAs of BLCAP (bladder cancer-associated protein) and IGFBP7 (insulin-like growth factor binding protein 7) demonstrated in total RNA extracted from the human cerebellum (d, lane 4) were not detected in either of the eluates (d).

### 2.4. Analyses for extents of A-to-I editing sites

Editing efficiencies at the A-to-I editing sites in GluR2, kv1.1 and CYFIP2 mRNAs were calculated by quantitative analyses of the digests of PCR products with restriction enzymes (Kawahara et al., 2003, 2004; Bhalla et al., 2004). The PCR products for GluR2 and kv1.1 were cleaved by BbvI (New England Biolabs, Ipswich, MA) and MfeI (New England Biolabs), respectively, and those for CYFIP2 were cleaved by MseI (New England Biolabs). Relative amounts of the resulting digests of PCR products were analyzed with a Bioanalyzer 2100 (Agilent Technologies, Santa Clara, CA). The extent of GluR2 Q/R site editing was calculated as the ratio of the molarity of the 129-bp band (derived from edited GluR2 mRNA) to the sum of the 129- and 91-bp bands (derived from unedited GluR2 mRNA). Similarly, the extent of kv1.1 I/V site editing was calculated as the ratio of the molarity of the 117-bp band (derived from edited kv1.1 mRNA) to the sum of the 117- and 66-bp bands (derived from unedited kv1.1 mRNA). The extent of CYFIP2 K/E site editing was calculated as the ratio of the molarity of the 216-bp band (derived from edited CYFIP2 mRNA) to the sum of those of both the 216- and 60-bp bands (derived from unedited CYFIP2 mRNA). Editing efficiencies at the A-to-I(G) editing sites in FLNA and BLCAP mRNAs were evaluated by sequencing the PCR products with a 3100 Genetic Analyzer sequencer (Applied Biosystems, Faster City, CA). Expression level of CYFIP2 mRNA was measured using a LightCycler System (Roche Diagnostics, Mannheim, Germany). The internal standards, primers, and probes for quantitative PCR for ADAR1, ADAR2 and CYFIP2 were designed as previously described (Kawahara et al., 2003) (Supplementary Table S1).

### 2.5. ADAR2 mRNA expression in human tissues

Quantitative PCR was performed using a LightCycler System (Roche Diagnostics, Indianapolis, IN), as described previously (Kawahara et al., 2003). Each cDNA human tissue sample was amplified in a reaction mixture (20 μl total volume) composed of 10 μl of 2× LightCycler 480 Probes Master Roche (Roche Diagnostics), 0.5 μM each primer, 0.1 μM probes (Universal ProbeLibrary Set, Human, #42 for ADAR2 and #64 for β-actin, Roche Diagnostics) (Supplementary Table S1).

### 2.6. Statistics

Differences between groups were evaluated using Student's *t*-tests. Differences were considered statistically significant at $P < 0.05$.

## 3. Results and discussion

### 3.1. mRNAs co-precipitated with ADAR2 in human brain

To identify mRNAs with ADAR2-mediated editing sites, we analyzed the ADAR2-immunoprecipitates of human cerebellum. First we confirmed that recombinant ADAR2 and Flag-ADAR2 proteins could be successfully immunoprecipitated with the E-20, and to a lesser extent with the C-15 antibodies against human ADAR2 peptides (Fig. 1a). As a second control of the method, immunoprecipitation using the E-20 antibodies was performed on nuclear extract of human cerebellum, and GluR2 and kv1.1 mRNAs, which were already known to have ADAR2-mediated editing sites, were selectively amplified from the RNA fraction of the complexes with RT-PCR (Fig. 1b; upper, middle). Thus, the natural substrates for ADAR2 should also be immunoprecipitable from human brain.

We found that CYFIP2 and FLNA mRNAs, but not BLCAP or IGFBP7 mRNAs, were specifically recovered from the ADAR2-precipitate (Fig. 1c and d), suggesting that CYFIP2 and FLNA mRNAs should have ADAR2-mediated editing sites. Then, we analyzed the A-to-I editing sites in kv1.1, CYFIP2, FLNA and GluR2 mRNAs extracted from cerebellar tissues and their ADAR2-immunoprecipitates. All CYFIP2 mRNAs recovered from the immunoprecipitates had U(G) instead of A at the predicted A-to-I editing position (K/E site) in genomic DNA (E.Y. Levanon et al., 2005), whereas 84% of the mRNA in the human cerebellar tissue was edited at this site (Fig. 2c and d). On the other hand, the previously reported A-to-I editing position (Q/R site) of FLNA mRNA (E.Y. Levanon et al., 2005) was edited to only 51% in the immunoprecipitate, and not to a detectable level in human cerebellum (Fig. 2e and f). In addition, the I/V site of kv1.1 mRNA was edited to a greater extent (36%) in the immunoprecipitate than in the cerebellar tissue (20%) (Fig. 2a and b), although the Q/R site of GluR2 mRNA was fully edited in both the immunoprecipitate (data not shown) and the human cerebellum (Kawahara et al., 2003). These results suggest that ADAR2 seems to bind predominantly to these mRNAs with ADAR2-mediated editing positions, more efficiently when these sites were edited than when unedited (Fig. 2a, c, e vs. b, d, f).

### 3.2. Editors at A-to-I positions in ADAR2-associated mRNAs

To determine whether ADAR2 specifically edits the putative editing sites of CYFIP2 and FLNA mRNAs but not BLCAP or IGFBP7 mRNAs, we investigated changes in the extent of RNA editing at these sites after knockdown of ADAR1 and ADAR2 using siRNAs (Supplementary Table S1) in HeLa cells. However, because the Q/R site in FLNA mRNA was not edited at all in HeLa cells (data not shown), and because the base sequence around the K/R site of IGFBP7-derived cDNA was GC-rich and was not suitable for sequencing analysis, we could determine the effects of siRNAs only at the K/E site of CYFIP2 and at the Y/C site of BLCAP mRNAs. Applications of siR1a and siR1b, to target ADAR1, and siR2a and siR2b, to target ADAR2, specifically and significantly decreased the copy numbers of ADAR1 and ADAR2 mRNAs, respectively (Fig. 3a and b). In addition, extent of GluR2 Q/R site editing was markedly decreased to nearly 0% after ADAR2 knockdown, but not significantly decreased after ADAR1 knockdown (data not shown), indicating that the knockdown of ADAR2 by this method sufficiently suppressed ADAR2 activity but not ADAR1 activity. Although the effects of ADAR1 knockdown could not be tested on natural substrates, previous studies have demonstrated that ADAR1 activity was significantly decreased with a similar method (Wong and Lazinski, 2002). The editing efficiencies at the CYFIP2 K/E site in HeLa cells were significantly reduced after applications of siR2a and siR2b (both $0.0 \pm 0.0\%$), and also, but to a lesser extent, after siR1a and siR1b, as compared to those after the application of siR n/c or normal culture medium alone (Fig. 3c). The results suggested that ADAR2 played a major role in RNA editing at this site, and ADAR1 may also have taken a part (Fig. 3b and c). On the other hand, sequence analysis of BLCAP mRNA-derived cDNA indicated that editing extent of the Y/C site of BLCAP mRNA was significantly lower after the application of

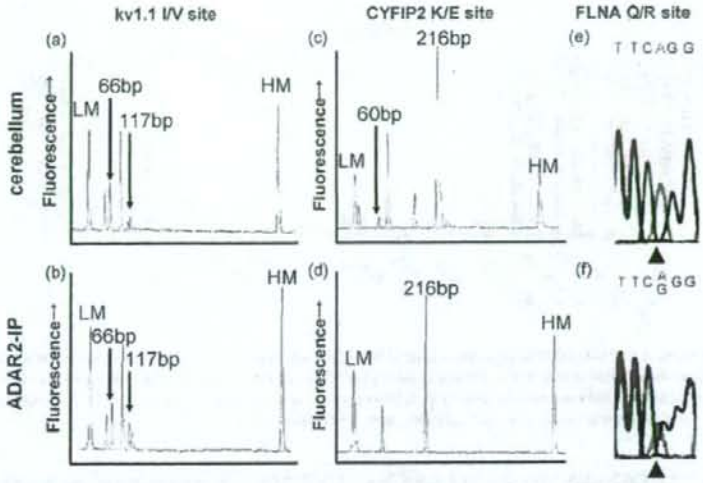


Fig. 2. Extent of editing in situ and in ADAR2-immunoprecipitates. The editing efficiency at the I/V site of kv1.1 mRNA was calculated as the ratio of the molarity of the 117-bp band (derived from edited kv1.1 mRNA) to the sum of those of both 117- and 66-bp bands (derived from unedited kv1.1 mRNA) after digestion of the PCR products with *MfeI*. Similarly, the editing efficiency at the K/E site of CYFIP2 mRNA was calculated as the ratio of the molarity of the 216-bp band (derived from edited CYFIP2 mRNA) to the sum of those of both the 216- and 60-bp bands (derived from unedited CYFIP2 mRNA) after digestion of the PCR products with *MseI*. (a, c and e) In the cerebellar tissue, extent of RNA editing was 20% at the kv1.1 I/V site (a), 84% at the CYFIP2 K/E site (c), and 0% at the FLNA Q/R site (G in e; arrowhead). (b, d and f) In the ADAR2-immunoprecipitates, on the other hand, extent of RNA editing was 36% at the kv1.1 I/V site (b), 100% at the CYFIP2 K/E site (d) and 51% at the FLNA Q/R site (G in f; arrowhead). LM, lower marker; HM, higher marker. Each value is the mean of two samples.

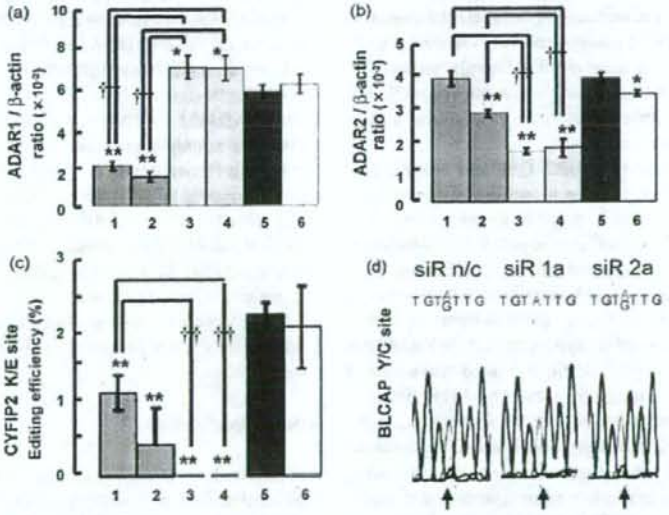


Fig. 3. Knockdown of ADAR1 and ADAR2. (a) The amount of ADAR1 mRNA relative to that of β-actin mRNA in HeLa cells was significantly decreased following knockdown treatment with siR1a and siR1b (1 and 2) but not with siR2a or siR2b (3 and 4). (b) The amount of ADAR2 mRNA relative to that of β-actin mRNA in HeLa cells was significantly decreased following knockdown treatment with siR2a and siR2b (3 and 4), compared to with siR1a or siR1b (1 and 2). (c) The editing efficiencies at the K/E site of CYFIP2 mRNA in HeLa cells were markedly decreased after ADAR2 knockdown (siR2a and siR2b, both 0.0 ± 0.0%), and to a lesser extent after ADAR1 knockdown (siR1a, 1.1 ± 0.2%; siR1b, 0.4 ± 0.5%), than control siRNA (siR n/c, 2.1 ± 0.2%; normal medium alone, 1.9 ± 0.5%). Each bar represents the value after administration of siRNA (mean ± S.D.; $n = 3$). Bar 1, siR1a; Bar 2, siR1b; Bar 3, siR2a; Bar 4, siR2b; Bar 5, siR negative control (n/c); Bar 6, no siR (Student's *t*-test, $^{*}P < 0.05$ and $^{**}P < 0.01$ vs. siR n/c and $^{\dagger\dagger}P < 0.01$ between bars as shown). (d) The sequence chromatography of the peaks at the Y/C site of BLCAP mRNA after the application of siR n/c (negative control, left), siR1a (ADAR1 knockdown, middle) or siR2a (ADAR2 knockdown, right). These demonstrate the lower peak of G at the Y/C site of BLCAP mRNA (arrows) after ADAR1 knockdown (siR1a, 2%; siR1b, 0%) than after ADAR2 knockdown (siR2a, 18%; siR2b, 16%) or control siRNA (siR n/c, 17%; normal medium alone, 13%). Each value is calculated as the mean of two samples.

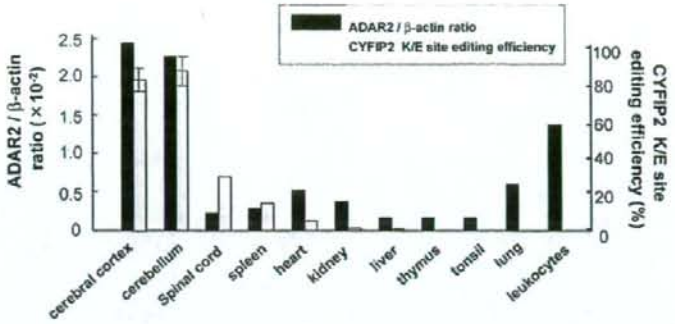


Fig. 4. CYFIP2 mRNA-editing extent and ADAR2 mRNA expression level in human tissues. Tissues with high expression levels of ADAR2 mRNA in the β-actin mRNA base (black columns) tend to show higher extent of RNA editing at the CYFIP2 K/E site (gray columns) than those with low ADAR2 mRNA expression level, whereas some regions with high ADAR2 mRNA expression level (e.g. leukocytes) showed very low extents of CYFIP2 mRNA editing. (Value represents the mean ± S.D. for multiple samples of cerebral cortex ($n = 4$), cerebellum ($n = 5$) and leukocytes ($n = 7$).)

ADAR1 siRNAs than after ADAR2 siRNAs or control siRNA (siR n/c and normal culture medium alone) (Fig. 3d). These results suggest that the Y/C site of BLCAP mRNA was edited predominantly with ADAR1 (Fig. 3d). Together with the results of immunoprecipitation (Fig. 1b–d), it seems likely that only mRNAs that have ADAR2-mediated editing positions form a complex with ADAR2.

The majority of A-to-I editing sites were localized in the non-coding regions particularly in the repetitive sequences within *Alu* and long interspersed element (LINE) sequences (K. Levanon et al., 2005) but the editors responsible for these sites have been only sporadically demonstrated (Kawahara et al., 2007). BLCAP mRNA has a long dsRNA hairpin structure (E.Y. Levanon et al., 2005) similar to *Alu* sequence, which suggests ADAR1 as a possible editor of A-to-I editing sites frequently seen in *Alu* sequence.

ADAR2 specifically catalyzes GluR2 Q/R site editing in mammalian and human brains, and the reduction of its editing activity may play a causative role in death of motor neurons in sporadic ALS patients (Kwak and Kawahara, 2005). Therefore knowledge about the regulatory mechanism of ADAR2 activity may promote our understanding of ALS pathogenesis. However, GluR2 Q/R site editing is always complete in neurons, and is somewhat reduced only when the expression of ADAR2 mRNA is reduced to a certain threshold level in human white matter (Kawahara et al., 2003), hence editing extents at this site may remain 100% when the reduction of ADAR2 activity was mild. On the other hand, CYFIP2 mRNA is ubiquitously expressed with the K/E site edited to variable extents among human tissues, especially abundant in the nervous system and lymphocytes (Mayne et al., 2004; Affymetrix HG-U133A: 215785_s_at). In this study, editing efficiencies at the CYFIP2 K/E site were $80.3 \pm 6.0\%$ in the cerebral cortex, $85.0 \pm 8.4\%$ in the cerebellum, 28.8% in the spinal cord, 14.5% in the spleen, 5.1% in the heart, and less than 1.5% in the other tissues. In addition, we found that the expression level of ADAR2 mRNA relative to that of β-actin mRNA was higher in the cerebral cortex ($2.49 \times 10^{-2}$) and the cerebellum ($2.30 \times 10^{-2}$) with high CYFIP2 K/E site-editing efficiency than in tissues with low CYFIP2 K/E site-editing efficiency (from $6.12 \times 10^{-3}$ in the lung to $1.66 \times 10^{-3}$ in the tonsil) (Fig. 4). However, CYFIP2 K/E site editing was inactive in the leukocytes and the lung in which ADAR2 mRNA expression was higher than in the spinal cord and the spleen where CYFIP2 K/E site editing was active (Fig. 4).

Consistent with the results of the knockdown experiment, there was a rough correlation between the CYFIP2 K/E site editing and ADAR2 mRNA expression. However, this correlation was less clear in some tissues such as leukocyte, suggesting the participation of certain unidentified tissue-specific ADAR2-regulatory factor(s) other than the expression level of ADAR2 mRNA. Indeed, ADAR2 mRNA-self-editing produced an mRNA isoform with premature stop codon in rat and mouse (Rueter et al., 1999; Feng et al., 2006), and protein-coding ADAR2 mRNA variants accounted for a small proportion among more than 48 splicing variants in human cerebellum (Kawahara et al., 2005). These results indicate that the total amount of ADAR2 mRNA may not directly correlate with that of active ADAR2 proteins. Furthermore expression level of ADAR1 may influence the ADAR2 activity by forming inactive heterodimers with ADAR2 (Centi et al., 2008).

Extent of editing at the CYFIP2 mRNA K/E site, a novel ADAR2-mediated A-to-I editing site, might become a potential marker for ADAR2 activity and hence a potential tool for ALS research.

## Acknowledgements

This study was supported in part by a Grant-in-Aid for Scientific Research from the Ministry of Health, Labor, and Welfare of Japan (H18-Kokoro-017, SK) and from the Ministry of Education, Culture, Sports, Science, and Technology of Japan (18023012, SK). We are grateful for the technical assistance of Ms. K. Ito, Ms. C. Tadami, and Ms. T. Tanaka.

## Appendix A. Supplementary data

Supplementary data associated with this article can be found, in the online version, at doi:10.1016/j.neures.2008.02.009.

## References

"Affymetrix HG-U133A: 215785_s_at" on the website http://symatlas.gnf.org (informations about CYFIP2 mRNA expression).

Bass, B.L., 2002. RNA editing by adenosine deaminases that act on RNA. Annu. Rev. Biochem. 71, 817–846.

Bhalla, T., Rosenthal, J.J., Holmgren, M., Reenan, R., 2004. Control of human potassium channel inactivation by editing of a small mRNA hairpin. Nat. Struct. Mol. Biol. 11, 950–956.

Brusa, R., Zimmermann, F., Koh, D.S., Feldmeyer, D., Gass, P., Seeburg, P.H., Sprengel, R., 1995. Early-onset epilepsy and postnatal lethality associated with an editing-deficient GluR-B allele in mice. Science 270, 1677–1680.

Burns, C.M., Chu, H., Rueter, S.M., Hutchinson, L.K., Canton, H., Sanders-Bush, E., Emeson, R.B., 1997. Regulation of serotonin-2C receptor G-protein coupling by RNA editing. Nature 387, 303–308.

Centi, C., Barzotti, R., Galeano, F., Corbelli, S., Rota, R., Massimi, L., Rocco, C.D., O'Connell, M.A., Gallo, A., 2008. Down-regulation of RNA editing in pediatric astrocytomas: ADAR2 editing activity inhibits cell migration and proliferation. J Biol Chem. 283, 7251–7260.

Feng, Y., Sansam, C.L., Singh, M., Emeson, R.B., 2006. Altered RNA editing in mice lacking ADAR2 autoregulation. Mol. Cell Biol. 26, 480–488.

Higuchi, M., Maas, S., Single, F.N., Hartner, J., Rozov, A., Burnashev, N., Feldmeyer, D., Sprengel, R., Seeburg, P.H., 2000. Point mutation in an AMPA receptor gene rescues lethality in mice deficient in the RNA-editing enzyme ADAR2. Nature 406, 78–81.

Kawahara, Y., Ito, K., Sun, H., Kanazawa, I., Kwak, S., 2003. Low editing efficiency of GluR2 mRNA is associated with a low relative abundance of ADAR2 mRNA in white matter of normal human brain. Eur. J. Neurosci. 18, 23–33.

Kawahara, Y., Ito, K., Sun, H., Aizawa, H., Kanazawa, I., Kwak, S., 2004. Glutamate receptors: RNA editing and death of motor neurons. Nature 427, 801.

Kawahara, Y., Ito, K., Ito, M., Tsuji, S., Kwak, S., 2005. Novel splice variants of human ADAR2 mRNA: skipping of the exon encoding the dsRNA-binding domains, and multiple C-terminal splice sites. Gene 363, 193–201.

Kawahara, Y., Zinshteyn, B., Sethupathy, P., Iizasa, H., Hatzigeorgiou, A.G., Nishikura, K., 2007. Redirection of silencing targets by adenosine-to-inosine editing of miRNAs. Science 315, 1137–1140.

Keegan, L.P., Gallo, A., O'Connell, M.A., 2001. The many roles of an RNA editor. Nat. Rev. Genet. 2, 869–878.

Kwak, S., Kawahara, Y., 2005. Deficient RNA editing of GluR2 and neuronal death in amyotropic lateral sclerosis. J. Mol. Med. 83, 110–120.

Levanon, E.Y., Hallegger, M., Kinar, Y., Shemesh, R., Djinovic-Carugo, K., Rechavi, G., Jantsch, M.F., Eisenberg, E., 2005. Evolutionarily conserved human targets of adenosine to inosine RNA editing. Nucleic Acids Res. 33, 1162–1168.

Levanon, K., Eisenberg, E., Rechavi, G., Levanon, E.Y., 2005. Letter from the editor: adenosine-to-inosine RNA editing in Alu repeats in the human genome. EMBO Rep. 6, 831–835.

Maas, S., Rich, A., Nishikura, K., 2003. A-to-I RNA editing: recent news and residual mysteries. J. Biol. Chem. 278, 1391–1394.

Mayne, M., Moffatt, T., Kong, H., McLaren, P.J., Fowke, K.R., Becker, K.G., Namaka, M., Schenck, A., Bardoni, B., Bernstein, C.N., Melanson, M., 2004. CYFIP2 is highly abundant in CD4+ cells from multiple sclerosis patients and is involved in T cell adhesion. Eur. J. Immunol. 34, 1217–1227.

Ohlson, J., Enstero, M., Sjoberg, B.M., Ohman, M., 2005. A method to find tissue-specific novel sites of selective adenosine deamination. Nucleic Acids Res. 33, e167.

Rueter, S.M., Dawson, T.R., Emeson, R.B., 1999. Regulation of alternative splicing by RNA editing. Nature 399, 75–80.

Takuma, H., Kwak, S., Yoshizawa, T., Kanazawa, I., 1999. Reduction of GluR2 RNA editing, a molecular change that increases calcium influx through AMPA receptors, selective in the spinal ventral gray of patients with amyotrophic lateral sclerosis. Ann. Neurol. 46, 806–815.

Wang, Q., Khillan, J., Gadue, P., Nishikura, K., 2000. Requirement of the RNA editing deaminase ADAR1 gene for embryonic erythropoiesis. Science 290, 1765–1768.

Wong, S.K., Lazinski, D.W., 2002. Replicating hepatitis delta virus RNA is edited in the nucleus by the small form of ADAR1. Proc. Natl. Acad. Sci. U.S.A. 99, 15118–15123.

OBSERVATION

# Lymphomatoid Granulomatosis Involving Central Nervous System Successfully Treated With Rituximab Alone

*Hiroyuki Ishiura, MD; Masato Morikawa, MD; Masashi Hamada, MD; Takuro Watanabe, MD, PhD; Shinichi Kako, MD; Shigeru Chiba, MD, PhD; Toru Motokura, MD, PhD; Akira Hangaishi, MD, PhD; Junji Shibahara, MD, PhD; Masaaki Akahane, MD, PhD; Jun Goto, MD, PhD; Shin Kwak, MD, PhD; Mineo Kurokawa, MD, PhD; Shoji Tsuji, MD, PhD*

**Objective:** To report the successful treatment of a patient with lymphomatoid granulomatosis (LYG), a rare Epstein-Barr virus–positive lymphoproliferative disorder, using rituximab (anti-CD20 monoclonal antibody). The prognosis for LYG has been reported to be poor, and no satisfactory treatment has been established. Because central nervous system (CNS) involvement of LYG has been known to show poor prognosis, the establishment of an effective treatment for CNS LYG with mild adverse effects is desired.

**Design:** Case report.

**Setting:** University hospital.

**Patient:** A 48-year-old Japanese man presenting with slowly progressive spastic paraparesis diagnosed as LYG involving the CNS and lungs.

**Interventions:** The patient was treated with rituximab (375 mg/m$^2$, once weekly for 1 month) alone.

**Main Outcome Measure:** Improvement of the lesions on imaging.

**Results:** The neurological signs resolved and the lesions in the CNS and lungs were mostly diminished after the rituximab monotherapy without any adverse effects. The patient stayed in remission for 18 months.

**Conclusion:** Rituximab monotherapy was effective in treating the patient; hence, rituximab should be considered as the initial treatment against LYG involving the CNS.

*Arch Neurol. 2008;65(5):662-665*

**Author Affiliations:**
Departments of Neurology (Drs Ishiura, Hamada, Goto, Kwak, and Tsuji), Hematology and Oncology (Drs Morikawa, Watanabe, Kako, Chiba, Motokura, Hangaishi, and Kurokawa), Pathology (Dr Shibahara), and Radiology (Dr Akahane), Graduate School of Medicine, The University of Tokyo, Tokyo, Japan.

LYMPHOMATOID GRANULOMATOSIS (LYG) is a rare lymphoproliferative disorder characterized by angiocentric and angiodestructive Epstein-Barr virus (EBV)–positive B-cell proliferation associated with extensive reactive T-cell infiltration.[1] The common sites of involvement include the lungs, skin, and central nervous system (CNS). To date, no satisfactory treatment has been established and treatments using corticosteroids, chemotherapy, interferon alfa-2b, radiotherapy, and stem cell transplantation have been selected according to patients' conditions.[1] The prognosis of LYG is generally poor, because some may evolve to EBV-positive diffuse large B-cell lymphoma. After the involvement of EBV-positive B cells had been established as essential in LYG development, a few reports on treatment with rituximab (a chimeric anti-CD20 monoclonal antibody) were published[1-4]; however, the outcome of this treatment for LYG involving the CNS is still undetermined. We herein report a case of LYG involving the CNS and lungs successfully treated with rituximab alone.

## REPORT OF A CASE

A 48-year-old man with well-controlled asthma and atopic dermatitis felt pain in both his shoulders 2 years and 9 months before his admission to our hospital. The pain gradually extended to his back and knees. Two years before his admission, he felt weakness in his knees. Eight months before his admission, he started to show gait disturbance. Numbness appeared in his toes on both feet and subsequently spread to his knees. Four months before his admission, he developed bladder in-

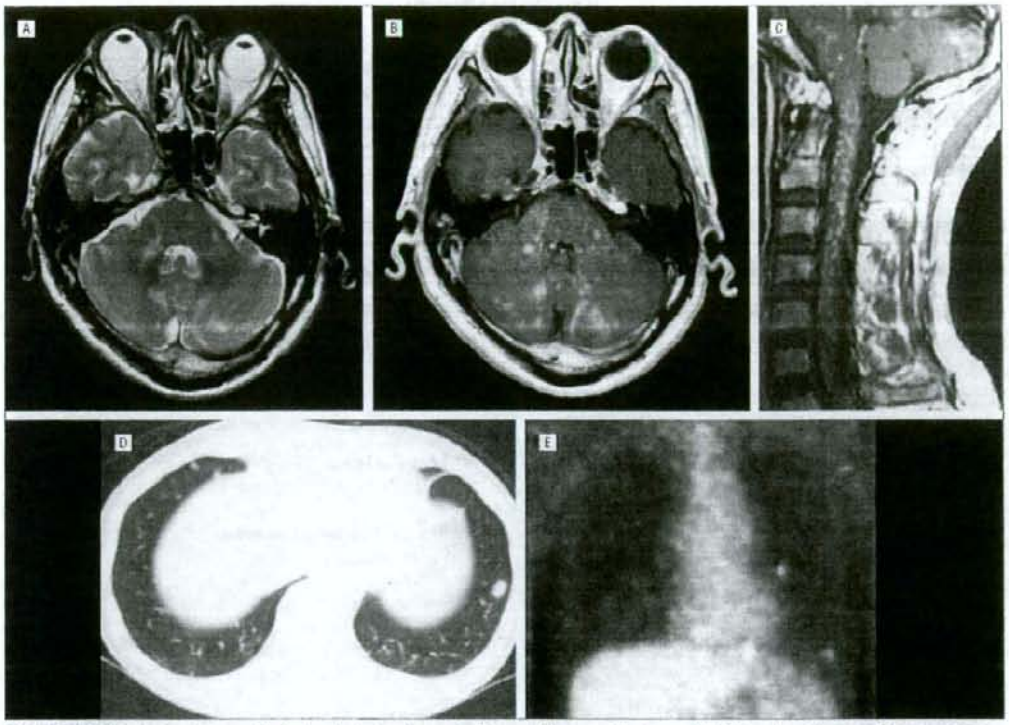


**Figure 1.** Magnetic resonance images of the head and spinal cord, computed tomographic scans of the lung, and [$^{18}$F]-fluorodeoxyglucose positron emission tomography (FDG-PET) of the body before treatment. A, Numerous spotty high-intensity lesions are observed in the pons and cerebellum on a T2-weighted image. B, These lesions are enhanced with gadolinium on a T1-weighted image. The lesions are also observed in the cerebral cortex to a lesser extent. C, A T1-weighted image with gadolinium enhancement of the cervical cord also demonstrates similar lesions. D and E, Nodular lesions are observed in the left lower lung and these lesions show abnormal FDG uptake, for which the maximum standard uptake value is 3.2.

continence. His gait worsened and he started to need a cane.

On admission to our hospital, his physical examination results were unremarkable except for atopic dermatitis. Neurological examination revealed spastic paraparesis with increased tendon reflexes in all his extremities and positive finger flexor reflexes. His plantar reflexes were extensor. He also had distal dominant dysesthesia of his lower limbs, spastic-type neurogenic bladder, and fecal incontinence. He was not able to run or go up the stairs. He could only walk with a cane for a short distance.

His serum soluble IL-2 receptor level was 550 U/mL (reference range, 167-497 U/mL). Anti–human immunodeficiency virus antibodies were not detected. His other laboratory results were unremarkable. His cerebrospinal fluid showed an elevated protein level (0.097 g/dL [to convert to grams per liter, multiply by 10]) and lymphocytic pleocytosis (28 cells/μL). The cytologic analysis showed no malignant cells. The test results for bacteria, *Mycobacterium tuberculosis*, and fungi were negative.

His nerve conduction study results, auditory brainstem response, and visually evoked potentials were normal. Short-latency sensory evoked potentials of the right tibial nerve revealed slight elongation of central conduction time (19.6 milliseconds), but those of the left tibial nerve were normal.

Magnetic resonance imaging of his head and spinal cord demonstrated numerous spotty lesions with a marked gadolinium enhancement (**Figure 1** A-C). Computed tomographic scans revealed nodular lesions in both his lungs, parts of which showed increased uptake rates of [$^{18}$F]-fluorodeoxyglucose (FDG) by positron emission tomography (Figure 1D and E). Video-assisted thoracoscopic biopsy of his left lung revealed infiltrates predominantly composed of lymphocytes. Immunohistochemical staining for CD3 and CD20 showed the predominance of T cells and a few B cells, respectively. In situ hybridization revealed positivity for the EBV-encoded viral RNA in a few lymphocytes (**Figure 2**), confirming the diagnosis of grade 1-2 LYG.

Although various therapeutic options, including whole-brain irradiation, were considered, we thought that less toxic therapeutic approaches were more appropriate for grade 1-2 LYG. Because the neoplastic B cells expressed CD20, the patient was treated with rituximab (375 mg/m$^2$, once weekly) for 4 weeks. Magnetic resonance images of his head and spinal cord showed marked im-

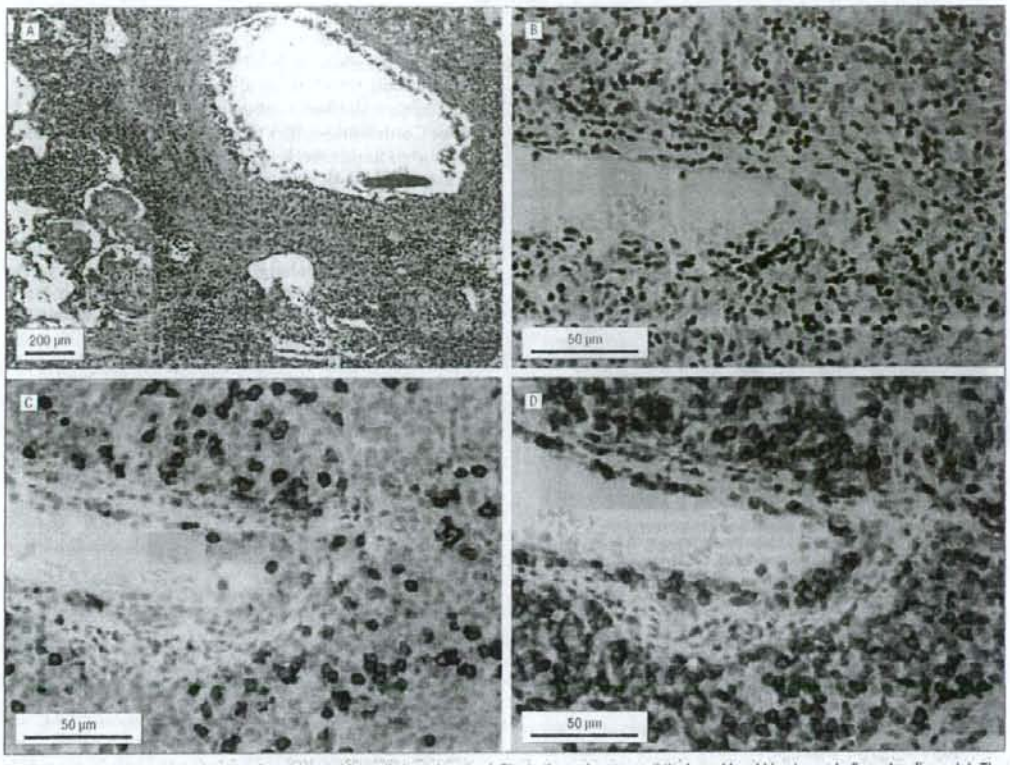


**Figure 2.** Histopathologic examination of the lung specimen. A, Lymphocytes infiltrate the regions around the bronchi and blood vessels (hematoxylin-eosin). The infiltrates are predominantly small lymphocytes admixed with histiocytes and occasionally large, atypical lymphoid cells, which are angiocentric and angioinvasive, thus destroying the blood vessels. B, Some of the lymphocytes are positive for Epstein-Barr virus–encoded viral RNA. C and D, CD20-positive B cells (C) are surrounded by a large number of CD3-positive T cells (D).

provement of the lesions 1 month after the treatment (**Figure 3**A and B) compared with the lesions in the images obtained before the treatment (Figure 1B and C), followed by further improvement of the lesions 8 months after the treatment (Figure 3C and D). The lesions in the lungs were hardly detected in the computed tomography scans 4 months after the treatment. His pain in his shoulders, back, and hips disappeared. His gait improved and he was able to walk without a cane for several hundred meters. For 18 months, his condition remained stable without recurrence.

## COMMENT

In this patient presenting with slowly progressive spastic paraparesis, numerous spotty lesions were observed in the CNS and lungs. The lesions showed contrast enhancement with gadolinium and FDG accumulation, and biopsy of the lesions in the left lung confirmed the diagnosis of LYG.

The definitive diagnosis of LYG is difficult, partly because of its rarity. The radiographic findings of the patient showing numerous granulomatous lesions in the CNS and lungs are highly suggestive of LYG[5] (Figure 1). [$^{18}$F]-fluorodeoxyglucose accumulation in these lesions further confirmed the diagnosis.[3]

A characteristic clinical feature of the patient was mild neurological signs of spastic paraparesis (he could walk even on admission) despite the striking radiographic findings. Consistent with mild neurological signs, only mild deteriorations in electrophysiological studies were observed in the patient. Such features are sometimes observed, for instance, in miliary tuberculosis involving the CNS. These features can also suggest the possibility of LYG.

Although the prognosis of LYG is variable, the median survival of patients with LYG has been shown to be less than 2 years, and CNS involvement, observed in about 30% of patients with LYG,[1] indicates poor prognosis. Although aggressive therapies, including chemotherapy, radiotherapy, and stem cell transplantation, have been conducted, no satisfactory standard treatment has been established for the treatment of LYG. Epstein-Barr virus–positive B-cell infiltration has been established as a pathognomonic feature of LYG. Since then, several reports on treatments with rituximab, with or without

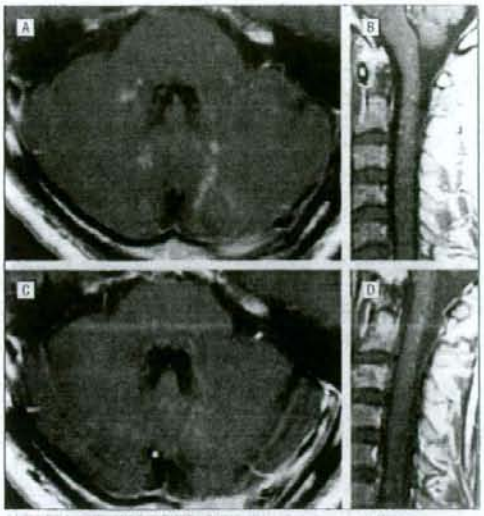


**Figure 3.** T1-weighted images with gadolinium enhancement of the cerebellum, pons, and cervical cord after treatment. A and B, The pons (A) and cerebellum (B) 1 month after treatment. C and D, The pons (C) and cerebellum (D) 8 months after treatment.

chemotherapy or radiotherapy, have been made.[1-4] Only 1 report on a patient with CNS LYG treated with rituximab alone[3] showed clinical remission for more than 36 months. Although approximately 1% of rituximab seems to pass through the blood-brain barrier and the effects of rituximab on CNS lesions are disputable,[6] our patient responded well to rituximab therapy without any adverse effects and his condition remained stable for 18 months, thus strongly suggesting the efficacy of rituximab monotherapy as the initial therapy for low-grade CNS LYG.

**Accepted for Publication:** September 16, 2007.
**Correspondence:** Shoji Tsuji, MD, PhD, Department of Neurology, Graduate School of Medicine, The University of Tokyo, 7-3-1 Hongo, Bunkyo-ku, Tokyo 113-8655, Japan (tsuji@m.u-tokyo.ac.jp).
**Author Contributions:** Drs Ishiura and Morikawa equally contributed to this work. *Study concept and design:* Ishiura, Hamada, Kwak, and Tsuji. *Acquisition of data:* Ishiura, Morikawa, Hamada, Watanabe, Kako, Shibahara, Akahane, Goto, Kwak, Kurokawa, and Tsuji. *Analysis and interpretation of data:* Ishiura, Hamada, Chiba, Motokura, Hangaishi, Shibahara, Akahane, Goto, Kwak, and Tsuji. *Drafting of the manuscript:* Ishiura, Morikawa, Hamada, Goto, Kwak, and Tsuji. *Critical revision of the manuscript for important intellectual content:* Hamada, Watanabe, Kako, Chiba, Motokura, Hangaishi, Shibahara, Akahane, Goto, Kwak, Kurokawa, and Tsuji. *Obtained funding:* Morikawa and Goto. *Administrative, technical, and material support:* Shibahara, Akahane, Kwak, and Tsuji. *Study supervision:* Hamada, Watanabe, Hangaishi, Goto, Kwak, Kurokawa, and Tsuji.
**Financial Disclosure:** None reported.

## REFERENCES

1. Rao R, Vugman G, Leslie WT, Loew J, Venugopal P. Lymphomatoid granulomatosis treated with rituximab and chemotherapy. *Clin Adv Hematol Oncol*. 2003; 1(11):658-660.
2. Sebire NJ, Haselden S, Malone M, Davies EG, Ramsay AD. Isolated EBV lymphoproliferative disease in a child with Wiskott-Aldrich syndrome manifesting as cutaneous lymphomatoid granulomatosis and responsive to anti-CD20 immunotherapy. *J Clin Pathol*. 2003;56(7):555-557.
3. Zaidi A, Kampalath B, Peltier WL, Vesole DH. Successful treatment of systemic and central nervous system lymphomatoid granulomatosis with rituximab. *Leuk Lymphoma*. 2004;45(4):777-780.
4. Jordan K, Grothey A, Grothe W, Kegel T, Wolf HH, Schmoll HG. Successful treatment of mediastinal lymphomatoid granulomatosis with rituximab monotherapy. *Eur J Haematol*. 2005;74(3):263-266.
5. Patsalides AD, Atac G, Hedge U, et al. Lymphomatoid granulomatosis: abnormalities of the brain at MR imaging. *Radiology*. 2005;237(1):265-273.
6. Rubenstein JL, Combs D, Rosenberg J, et al. Rituximab therapy for CNS lymphomas: targeting the leptomeningeal compartment. *Blood*. 2003;101(2):466-468.

THE JOURNAL OF COMPARATIVE NEUROLOGY 511:155–172 (2008)

# High-Affinity $Na^+/K^+$-Dependent Glutamate Transporter EAAT4 Is Expressed Throughout the Rat Fore- and Midbrain

ANN MASSIE,[1] LIESELOTTE CNOPS,[2] ILSE SMOLDERS,[1] ROBERT McCULLUMSMITH,[3] RON KOOIJMAN,[4] SHIN KWAK,[5] LUTGARDE ARCKENS,[2] AND YVETTE MICHOTTE[1]*

[1]Department of Pharmaceutical Chemistry and Drug Analysis, Research Group of Experimental Pharmacology, Vrije Universiteit Brussel, 1090 Brussels, Belgium
[2]Laboratory of Neuroplasticity and Neuroproteomics, Katholieke Universiteit Leuven, 3000 Leuven, Belgium
[3]Department of Psychiatry, University of Alabama at Birmingham, Birmingham, Alabama 35294
[4]Department of Pharmacology, Vrije Universiteit Brussel, 1090 Brussels, Belgium
[5]Department of Neurology, Division of Neuroscience, Graduate School of Medicine, University of Tokyo, Tokyo 113, Japan

ABSTRACT

Excitatory amino acid transporter 4 (EAAT4), a member of the high-affinity $Na^+/K^+$-dependent glutamate transporter family, is highly enriched in Purkinje cells of the cerebellum, although it is not restricted to these cells. The detailed expression of EAAT4 protein in different adult rat fore- and midbrain regions was examined. Despite moderate expression levels compared with the cerebellum, EAAT4 protein was omnipresent throughout the fore- and midbrain. With antibodies raised against the N-terminal mouse EAAT4 sequence, the highest protein expression levels were observed in the substantia nigra pars compacta, ventral tegmental area, paranigral nucleus, habenulo-interpeduncular system, supraoptic nucleus, lateral posterior thalamic nucleus, subiculum, and superficial layers of the superior colliculus. Relatively high levels of EAAT4 protein were also detected in the hippocampal principal cells, in the glutamatergic, γ-aminobutyric acid (GABA)ergic, dopaminergic and most likely cholinergic cells of all nuclei of the basal ganglia, and in neurons of layers II/III and V of the cerebral cortex. The expression of EAAT4 was confirmed at the mRNA level in some important fore- and midbrain structures by in situ hybridization and reverse transcriptase-polymerase chain reaction (RT-PCR) and estimated to range from 6.7 to 1.6% of the amount in the cerebellum as measured by real-time PCR. J. Comp. Neurol. 511:155–172, 2008. 

**Indexing terms: EAAT4; fore- and midbrain; distribution; immunohistochemistry; real-time PCR; in situ hybridization**

High-affinity $Na^+/K^+$-dependent glutamate transporters are responsible for the reuptake of synaptically released glutamate, the major excitatory neurotransmitter in the central nervous system (CNS), into glial cells or neurons. Five different excitatory amino acid transporters (EAATs) have been cloned so far (Saier, 1999; Slotboom et al., 1999): GLAST (Storck et al., 1992; Tanaka, 1993), GLT-1 (Pines et al., 1992), and EAAC1 (Kanai and Hediger, 1992), corresponding to human EAAT1, -2, and -3, respectively, EAAT4 (Fairman et al., 1995), and EAAT5 (Arriza et al., 1997). Through the proper functioning of these glutamate transporters, glutamatergic neurotransmission is carefully regulated and excitotoxicity is prevented (for review, see Danbolt, 2001). This regulation also includes control over the extent of glutamate spillover and ensuing activation of extrasynaptic targets at excita-

Grant sponsor: FWO-Flanders; Grant numbers: 1.5.143.07N, postdoctoral fellowships (to A.M. and I.S.), and research assistant (to L.C.); Grant sponsor: the Vrije Universiteit Brussel.

*Correspondence to: Yvette Michotte, Ph. D., Department of Pharmaceutical Chemistry and Drug Analysis, Research Group of Experimental Pharmacology, Vrije Universiteit Brussel, Laarbeeklaan 103, 1090 Brussels, Belgium. E-mail: ymichot@vub.ac.be

Received 21 December 2005; Revised 24 August 2006; Accepted 11 July 2008

DOI 10.1002/cne.21823

Published online in Wiley InterScience (www.interscience.wiley.com).

tory synapses (Bergles et al., 1999). In addition, glutamate transporters also behave as glutamate-gated chloride channels, a property that is particularly prominent in EAAT4 and EAAT5 (Fairman et al., 1995; Vandenberg et al., 1995; Wadiche et al., 1995a,b; Arriza et al., 1997; Torres-Salazar and Fahlke, 2007).

Originally, the five members of this transporter family were thought to have not only a distinct regional but also a distinct cellular distribution pattern. GLAST and GLT-1 were reported to be confined to glial cells (Rothstein et al., 1994; Torp et al., 1994; Chaudhry et al., 1995; Lehre et al., 1995). EAAC1 and EAAT4 were considered to be strict neuronal transporters (Rothstein et al., 1994; Yamada et al., 1996; Furuta et al., 1997). However, this interpretation was challenged by several reports, and it soon became clear that the subdivision of glutamate transporters into "glial" and "neuronal" was no longer tenable (however, for ease this subdivision is still generally used). GLT-1 is expressed in neurons of cortical and hippocampal culture (Mennerick et al., 1998; Wang et al., 1998). Also, in vivo, GLT-1, as well as its splice variants, can be expressed by neurons (Rauen and Kanner, 1994; Schmitt et al., 1996; Torp et al., 1996; Berger and Hediger, 1998; Berger et al., 2005; Chen et al., 2002, 2004). EAAT4 expression has been reported to be enriched in astrocytes of mouse spinal cord and forebrain (Hu et al., 2003) as well as in rat retinal astrocytes (Ward et al., 2004). Very recently, Liang et al. (2008) described the presence of the mRNA of all EAATs (i.e., EAAT1–5) in astrocyte cultures. Moreover, glia were reported to have the potential to upregulate EAAT4 after traumatic brain injury (Yi et al., 2007). EAAT5, thought to be primarily neuronal, is predominantly expressed in the retina (Arriza et al., 1997) and will therefore not be discussed in further detail.

As for the regional distribution pattern, GLAST immunoreactivity (IR) is known to be highly abundant in cerebellar Bergman glia (Lehre et al., 1995; Lehre and Danbolt, 1998; Attwell, 2000), whereas GLT-1, which is responsible for the bulk of glutamate removal, is highly expressed in astrocytes of the cerebral cortex and hippocampus (Lehre et al., 1995). EAAC1 expression within the CNS has been described in the cerebral cortex, hippocampus, and basal ganglia.

It is commonly accepted that EAAT4 is largely confined to Purkinje cells of the cerebellum, with little or no expression in forebrain regions (Yamada et al., 1996; Bar-Peled et al., 1997; Furuta et al., 1997; Itoh et al., 1997; Nagao et al., 1997; Tanaka et al., 1997; Dehnes et al., 1998; Inage et al., 1998). However, Furuta et al. (1997) have reported very low expression levels of EAAT4 protein in the forebrain and more particularly in the cerebral cortex, hippocampus, and some basal ganglia nuclei. Also, McCullumsmith and Meador-Woodruff (2002) detected EAAT4 mRNA in the striatum of human subjects. Recently, we described the expression of this glutamate transporter in more detail in neurons of the cerebral cortex of cat and mouse (Massie et al., 2001). The presence of EAAT4 in the cerebral cortex has been confirmed at the mRNA (Ward et al., 2004) as well as the protein level (Hu et al., 2003). Nevertheless, the expression level in the cerebral cortex has been estimated to be only approximately 3% that of the cerebellum (Ward et al., 2004). More recently, EAAT4 has also been described to be expressed in photoreceptors and astrocytes of the retina (Ward et al., 2004; Pignataro et al., 2005). Thus, it is becoming more and more clear that EAAT4 is more widespread in distribution than was initially thought. In addition, several recent studies report changes in the expression levels of EAAT4 mRNA and/or protein in various fore-and midbrain regions of various brain pathologies (McCullumsmith and Meador-Woodruff, 2002; Rakhade and Loeb, 2008; Yi et al., 2007).

To our knowledge, this is the first report describing in detail the cellular and regional distribution of EAAT4 protein and mRNA throughout the rat fore- and midbrain. By using an antibody raised against the N-terminal mouse EAAT4 sequence (Yamada et al., 1996), as well as a staining protocol ensuring optimal permeability of cells for the antibodies, EAAT4 protein could be clearly observed in neurons throughout the fore- and midbrain, notwithstanding the manifestly higher levels in the Purkinje cell layer of the cerebellum. In addition, the presence of EAAT4 mRNA in the fore-and midbrain was confirmed by using reverse-transcriptase-polymerase chain reaction (RT-PCR) and in situ hybridization. The expression level of EAAT4 mRNA relative to the cerebellum was determined for the cerebral cortex, hippocampus, and striatum by using real-time PCR.

## MATERIALS AND METHODS

### Animals

Protocols for animal experiments described in this study were carried out according to national guidelines on animal experimentation and were approved by the Ethical Committee for Animal Experimentation of the Faculty of Medicine and Pharmacy of the Vrije Universiteit Brussel.

All animals used for this study were housed under standard laboratory conditions. Eight adult male Wistar rats (weighing 250–275 g) were sacrificed for the immunohistochemical study, six for the Western blotting, and three for the RT-PCR and real-time PCR experiments.

Mice bearing heterozygous null mutations for EAAT4 were a gift of Dr. K. Tanaka (Huang et al., 2004). Breeding with these mice resulted in litters containing $EAAT4^{+/+}$, $EAAT4^{+/-}$, and $EAAT4^{-/-}$ mice. Four 12-week-old male mice of each genotype were used for this study.

### Western blotting

After rats or mice were injected with a lethal dose of pentobarbital, i.p. (Nembutal, Sanofi sante, Brussels, Belgium), brains were immediately dissected. A small tissue sample ($\pm 4$ $mm^3$) was collected from the cerebral cortex, striatum, hippocampus, and cerebellum, snap-frozen in dry ice-cooled 2-methylbutane (−60°C), and stored at 70°C until use.

Protein extraction and Western blotting were performed as described before (Massie et al., 2003). Tissue was homogenized in 2% sodium dodecyl sulfate (SDS; Polylab, Antwerp, Belgium), 60 mM Tris base (ICN Biomedicals, Aurora, OH), pH 6.8, 100 mM dithiothreitol (DTT; Merck Eurolab, Leuven, Belgium), and 1 mM EDTA (Merck Eurolab). After incubation for 30 minutes at 37°C, samples were processed four times through 20-gauge needles and then through a 26-gauge needle, spun at 10,000*g* at 4°C (Eliasof et al., 1998), and immediately boiled for 10 minutes. Supernatants were stored at 70°C. Protein concentrations were determined by using a modified Bradford method (Qu et al., 1997). Equal concentrations of protein

(1.6 μg/lane) were loaded for all forebrain regions; for the cerebellum, four times less protein was loaded.

Proteins were separated by SDS-polyacrylamide gel electrophoresis (PAGE; 4–12% gel; Invitrogen, Groningen, The Netherlands) under reducing conditions and transferred to a polyvinylidene fluoride membrane (Sequi-Blot PVDF Membrane, Bio-Rad Laboratories, Nazareth, Belgium) by using an Xcell II Blot module (Novex, Invitrogen). Nonspecific binding was blocked by incubating the membrane for 1 hour at room temperature in 5% dried milk (ECL blocking agent, GE Healthcare, Roosendaal, The Netherlands). Blots were incubated overnight at 4°C with the immunoaffinity-purified polyclonal antibodies to EAAT4, raised in rabbit against the N-terminal mouse sequence (MSSHGNSLFLRESGAGGGCL; 760 μg/ml; diluted 1:4,000; kindly provided by Dr. M. Watanabe; same batch as in Yamada et al., 1996). The next day, after incubation with horseradish-peroxidase-conjugated anti-rabbit antiserum (1:2,000; Dako, Glostrup, Denmark), immunoreactive proteins were visualized by using enhanced chemiluminescence (ECL; ECLplus kit, GE Healthcare). All washing and dilution steps were performed with Tris-saline (0.01 M, pH 7.4). The MultiMark Multi-Colored Standard (Novex, Invitrogen) was used as molecular weight standard. Negative controls included omission of the immunoaffinity-purified antibody and the secondary antibody, respectively.

## Immunohistochemistry

Rats or mice were deeply anesthetized with an overdose of Nembutal, i.p., and transcardially perfused with a physiological solution followed by freshly depolymerized 4% paraformaldehyde (Sigma-Aldrich, St. Louis, MO) in 0.15 M phosphate-buffered saline (PBS; pH 7.42). Brains were removed and postfixed in the same fixative overnight, rinsed in tap water for 24 hours, and stored in 0.015 M PBS at 4°C. Free-floating 50-μm frontal and sagittal sections were made with a vibratome and stored in serial order in 0.015 M PBS at 4°C.

All rinsing steps and incubations of the staining procedure were performed in Tris-saline (0.01 M, 0.05% Triton X-100 [Sigma-Aldrich], pH 7.4) or in 0.015 M PBS, always at room temperature, unless mentioned otherwise, and under gentle agitation. All results shown and discussed were obtained with the Triton X-100-containing staining protocol unless otherwise noted. Incubation steps were separated by three rinsing steps of at least 5 minutes. The sections underwent a permeabilizing treatment consisting of incubation in 0.1% trypsin (Fluka, Buchs, Switzerland) for 1 hour at 37°C prior to a blocking step with normal goat serum (Chemicon, Temecula, CA, diluted 1:5, 45 minutes). Thereafter the sections were incubated with the primary EAAT4 antibodies (diluted 1:2,000; Yamada et al., 1996) for 2 days. On the third day the sections were processed by the avidin-biotin method by using a Vectastain ABC kit (Vector, Burlingame, CA), and immunoreactivity was visualized, after a final rinsing step with acetate buffer, by using the glucose oxidase-diaminobenzidine-nickel method (Shu et al., 1988). Sections were mounted on poly-L-lysine-coated slides, dehydrated through alcohol, cleared with xylene, and coverslipped with Coverquick (Labonord, Templemars, France). Negative controls consisted of the omission of the primary and secondary antibodies, respectively.

Photomicrographs were made of the stained sections, and brightness and contrast were adapted by using Adobe Photoshop 7.0.

## Laser microdissection (LMD)

After the brain was snap-frozen, 14-μm sections were cut on a cryostat and mounted on home-made glasses that were covered with a poly-ethylene naphtalate (PEN) foil and exposed to UV radiation for 30 minutes prior to use. Glasses were placed in a Leica AS LMD system (Leica, Leitz Instruments, Heidelberg, Germany) with the section facing downward. After adjusting intensity, aperture, and cutting velocity, the pulsed UV laser beam was carefully directed along the borders of the fasciculus retroflexus of several serial sections by using the 4× objective. The area cut fell by forces of gravity alone into a plastic tube cap placed directly underneath the section. The tube cap was filled with lysis solution. Tissue collection was verified by inspecting the tube cap under higher magnification.

## RT-PCR

Total RNA was extracted from tissue samples of the fasciculus retroflexus, collected by the LMD technique, as well as manually isolated tissue samples from cryosections of the cerebellum, cerebral cortex, hippocampus, and striatum, by using the Versagene total RNA purification kit (Gentra Systems, Big Lake, MN). RT-PCR was performed according to the instructions of the manufacturer (GeneAmp® RNA PCR kit from Applied Biosystems, Foster City, CA). For the reverse transcription oligo(dT) primers were used. The EAAT4-specific primers used for PCR amplification were designed according to the known rat sequence of EAAT4 (GenEmbl. u89608; Lin et al., 1998; upstream primer: 5′-GGAGACTGTGCCTGTACCTGG-3′, downstream primer: 5′-GCAGAGCTGGAAGAGGTACCC-3′, corresponding to nucleotides 906–926 and 1,299–1,319 respectively; Eurogentec, Seraing, Belgium). A total of 40 reaction cycles (95°C 1 minute, 60°C 1 minute, 70°C 1 minute) was preceded by 1 cycle starting at 95°C for 10 minutes to activate the polymerase enzyme (AmpliTaq® Gold DNA polymerase, 2.5 U/100 μl; Applied Biosystems) and concluded by a termination step at 70°C for 10 minutes. As negative control the cDNA in the reaction mixture was substituted by water.

Amplified products were analyzed by horizontal agarose gel electrophoresis and visualized by ethidium bromide staining. A 100-bp ladder (Invitrogen) was used as molecular weight reference.

## Real-time PCR

Total RNA was extracted, and, after biophotometric analysis (Eppendorf, VWR International, Leuven, Belgium), RT was performed as described above on mRNA samples of identical quantity. Primers and probes were designed by using the Primer Express Program (Applied Biosystems), based on the rat sequence of EAAT4 (GenEmbl. u89608; forward primer: 5′-TTGCGCCTGCAGACCAT-3′; reverse primer: 5′-AGCGCTGACTGTGAGCAAGA-3′; Taqman probe: 5′-CGCTTCCTGCGCCGAAATGC-3′) and GAPDH (GenEmbl. NM017008; forward primer: 5′-TGCCTGGATCCCTAAAGAGACA-3′; reverse primer: 5′-CGCGATATTCAATTGGATACACA-3′; Taqman probe: 5′-CCATTTCCAAGACTGACAGCCCCAGA-3′). Primers were obtained from Eurogentec, and FAM-TAMRA Taqman probes were purchased from Applied Biosystems.

PCR was performed on the cDNA samples in a 25-µl reaction volume of 1× Taqman Universal PCR Master Mix (Applied Biosystems) with primers at a final concentration of 300 nM and probes of 200 nM, using the ABI Prism 7000 Sequence Detection System. Standard curves were generated by running serial dilutions (1:2) of control cDNA in duplicate for each gene. Target samples were run in triplicate on the same well-plate under standard amplification settings (1 cycle of 50°C for 2 minutes, 1 cycle of 95°C for 10 minutes, 40 cycles of 95°C for 15 seconds and 60°C for 1 minutes).

Data were analyzed with ABI Prism 7000 SDS software (version 1.1). EAAT4 quantities were normalized to GAPDH, an endogenous control, to account for variability in the initial concentration of mRNA in the samples and to compensate for differences in conversion efficiency of the RT reaction. Amounts of transcripts in the cerebral cortex, striatum, hippocampus, and fasciculus retroflexus were expressed relative to the cerebellum which was set as the calibrator (=100%). To confirm reproducibility, real-time PCR was performed twice on each rat (n = 3).

### In situ hybridization

After rats were injected with a lethal dose of Nembutal, i.p., brains were immediately dissected and snap-frozen in dry ice-cooled 2-methylbutane ( 60°C) and then stored at −80°C until use. In situ hybridization experiments were performed as described by McCullumsmith and Meador Woodruff (2002). To generate a subclone for riboprobe synthesis, we amplified a unique region of EAAT4 (U89608, 576–959) from a rat cDNA brain library (Edge-Biosystems, Gaithersburg, MD) by using PCR. Amplified cDNA segments were extracted (QIAquick Gel Extraction kit; Qiagen, Valencia, CA), subcloned (Zero Blunt TOPO PCR cloning kit; Invitrogen, Carlsbad, CA), and confirmed by nucleotide sequencing (Thermo Sequenase Radiolabeled Termination Cycle Sequencing kit; USB, Cleveland, OH). Riboprobes were synthesized by using 100 µCi of dried [$^{35}$S]-UTP, 2.0 µl 5X transcription buffer, 1.0 µl 0.1 M DTT, 1.0 µl each of 10 mM ATP, CTP, and GTP, 2.0 µl linearized plasmid DNA, 0.5 µl RNAse inhibitor, and 1.5 µl SP6 or T7 RNA polymerase, and incubated for 2 hours at 37°C. After this incubation, 1.0 µl DNAse (RNAse free) was added and incubated for 15 minutes at room temperature. The reaction mixture was separated through spin columns (Micro Bio-Spin P-30 Tris Chromatography Columns, Bio-Rad, Richmond, CA), and the purified fraction was eluted. DTT was added to each fraction to a final concentration of 0.01 M.

Slides were removed from −80°C storage, fixed in 4% (wt/vol) formaldehyde at room temperature for 1 hour, and briefly washed in 2X SSC (standard saline citrate: 300 mM NaCl/30 mM sodium citrate, pH 7.2) three times. The slides were then placed in 0.1 M triethanolamine (pH 8.0)/acetic anhydride (400:1 vol/vol) with stirring for 10 minutes at room temperature. The final wash was in 2X SSC buffer for 10 minutes followed by dehydration in graded ethanol washes and air drying. A coverslip containing the [$^{35}$S]-radiolabeled riboprobe diluted $5 \times 10^6$ cpm in 0.1 ml per slide of hybridization buffer (50% formamide, 10% dextran sulfate, 3X SSC, 50 mM $Na_2HPO_4$, pH 7.4, 1X Denhardt's solution [0.02% polyviny pyrrolidone, 1.02& Ficoll, 0.02% bovine serum albumin], 100 µg/ml yeast tRNA) and 0.01 M DTT was placed on each slide. Slides were then placed in a covered tray with filter paper saturated with 50% formamide buffer and incubated at 55°C overnight. Sense and antisense probes were tested to confirm specificity. After 16 hours of hybridization, the coverslips were removed and the slides were washed in 2X SSC for 2 minutes and again in 2X SSC for 15 minutes, and then immersed in RNAse A (200 µg/ml in 10 mM Tris-HCl pH 8.0/0.5 M NaCl) for 30 minutes at 37°C. The slides then underwent washes through descending concentrations of SSC, to a final concentration of 0.1X SSC at 55°C for 1 hour twice. Sections were finally dehydrated in graded ethanol washes, air-dried, and exposed to Kodak BIOMAX MR film (Kodak, Rochester, NY) for 3 months. All sections were run in the same experiments to eliminate interassay variability. Neighboring sections were stained with Richardson's methylene blue-azure II Nissl stain (Richardson et al., 1960). Digital photomicrographs of the Nissl-stained sections were made by using the Leica IM50 software. Brightness and contrast were adapted by using Adobe Photoshop 7.0.


Fig. 1. **A:** Western blot analysis with the EAAT4 antibodies on protein extracts from rat cerebellum (Cb), cerebral cortex (Cx), hippocampus (Hc), and striatum (Str). In each lane one band could be detected with a molecular weight of approximately 68 kDa. **B:** Western blotting on homogenates of cerebellar (Cb) and cerebral cortex (Fb) of EAAT4 heterozygous (+/ ) and homozygous ( /- ) mice and their wild-type (+/+) littermates. **C:** Immunohistochemical staining of frontal sections of EAAT4$^{+/+}$ and EAAT4$^{-/-}$ mouse brain by using the EAAT4 antibody. Scale bar 1 mm in C

## RESULTS

### Specificity of the antibodies

Western blotting was used to investigate the specificity of the antibody in recognizing EAAT4 in four principal rat brain regions. Proteins were extracted from the cerebral cortex (Cx), the striatum (Str), the hippocampus (Hc), and the cerebellum (Cb) of the rat. Incubation of the blotting membrane with the EAAT4 antibody that recognizes the N-terminus of EAAT4 resulted for all protein samples in the detection of a specific band with a molecular weight of approximately 68 kDa, corresponding to the molecular weight of EAAT4 (Fig. 1A).

We observed a difference of a few kDa between the molecular weight of the immunoreactive bands of the cerebellum and the forebrain regions, the latter being a few kDa higher than the former (Fig. 1A). However, exposing the light-sensitive film for a longer period of time to the membrane revealed a second band for the cerebellum with

the same molecular weight as the bands of the forebrain regions (data not shown). Because of the very high intensity of the lower band, these two bands appear as one broad and intense band. Possibly, the appearance of this double band can be explained by post-translational modifications, the higher band corresponding to a more glycosylated and/or phosphorylated form of EAAT4 (Massie et al., 2001). If phosphorylations are mostly localized to the N-terminus of the protein, it might make the epitope of the antibodies less accessible, explaining why this higher molecular weight band is less easily detected, compared with the lower molecular weight band. At the same time, this might explain why bands are faint and fuzzy in forebrain regions where we only detected this higher molecular weight band (Fig. 1A). For all conditions, when higher protein concentrations were loaded, a smear of higher molecular weight bands became noticeable. These bands have been described abundantly in the literature for EAAT4 (Hu et al., 2003) as well as for the other glutamate transporter subtypes (Danbolt et al., 1990; Haugeto et al., 1996) as being multimers of the transporter protein. Omitting the primary antibodies resulted in a blank lane (data not shown).

Specificity of the antiserum was further confirmed by Western blotting and immunohistochemistry on samples of the cerebellum and cerebral cortex of mice bearing heterozygous or homozygous null mutations for EAAT4 and their wild-type littermates. When comparing samples of cerebral cortex with the same amount of protein, the concentration of the 68 kDa band in the EAAT4$^{+/-}$ samples is markedly reduced compared with the wild-type samples, whereas in the EAAT4$^{-/-}$ mice this band is absent (Fig. 1B, lower arrow). Similar observations were made in the cerebellum, where the 68-kDa band was reduced in heterozygous mice and completely absent in EAAT4$^{-/-}$ mice. However, in EAAT4$^{+/-}$ and EAAT4$^{-/-}$ mice we detected immunoreactive bands with a molecular weight slightly higher than the 68-kDa band found in WT mice (Fig. 1B, upper arrow). This immunoreactive band was completely absent in the homogenates of their WT littermates.

We speculate that insertion of the neoTK targeting vector in the coding region of exon 8 leads to partial transcription of this vector and as a consequence the translation of low levels of a larger protein of which the N-terminal region is identical to the N-terminal part of EAAT4 and thus still recognized by the antibody. This idea is in line with the detection of a faint immunoreactive signal in forebrain slices of EAAT4$^{-/-}$ mice after immunohistochemical staining in comparison with EAAT4$^{+/+}$ mice (Fig. 1C). In samples of the cerebellum, the difference in concentration between the larger protein and the WT protein is much more pronounced, because the former is only visible after prolonged exposure of the membrane to the light-sensitive film (data not shown).

## Immunohistochemical distribution of EAAT4

*Overview.* In general, EAAT4-positive neurons could be detected throughout the whole rat brain, with the most intense staining in the cerebellum (Fig. 3C,D). In the fore- and midbrain (Figs. 3–6), the strongest signal was present in the subiculum (S), substantia nigra pars compacta (SNc), ventral tegmental area (VTA), medial habenular nucleus (MHb), fasciculus retroflexus, interpeduncular nucleus (IP), supraoptic nucleus, paranigral nucleus, lateral posterior thalamic nucleus (LPMC), and superficial and zonal layers of the superior colliculus (SC) (Figs. 4–6, Table 1). A relatively strong labeling could also be detected in layers II/III and V of the cerebral cortex (Fig. 3A,B), the principal cells of the hippocampal formation (Fig. 4), and the basal ganglia (Fig. 6, Table 1).

Overall, when Triton X-100 was included in rinsing and incubation steps (Tris-saline or PBS + 0.3% Triton), immunopositive neurons were much more abundantly present compared with staining without Triton (rinsing and incubation with PBS) (Fig. 3A,B). Moreover, in sections treated with Triton X-100, EAAT4-IR was clearly present in the cytoplasm (Figs. 2, 3B). This finding suggests that the antigenic sites in the cytoplasm are less reachable compared with those from EAAT4 proteins in cell membranes and dendrites. Conversely, in accordance with the observations of Dehnes et al. (1998), in the cerebellar Purkinje cells, we detected intracellular staining without Triton X-100, probably because of the higher concentrations of EAAT4 in the cerebellum compared with the fore- and midbrain. As was proposed for EAAC1, this deviating localization might imply that EAAT4 can be rapidly mobilized from the cytoplasm to the plasma membrane, resulting in rapid changes in EAAT4-surface expression near the synapse (Davis et al., 1998; Conti et al., 1998; Kugler and Schmitt, 1999).

Besides the intense somatodendritic labeling, which manifests as a uniform dark staining, we could also detect a punctate or granular staining (Fig. 2). This granular staining is prominent in the neuropil and dendrites but also in the cell bodies. Some cell bodies are defined only by these granules (Fig. 2D,E), whereas others show a dark homogeneous staining of some parts of the cell body or the whole cell body and are additionally covered by these granules (Fig. 2C).

In general, glial labeling was very faint and could be observed in several white matter regions of the brain, in ependymal cells and tanycytes lining the lateral and third ventricle as well as in the choroid plexus (Table 1). The typical arrangement of the glial cells in rows, as observed in the corpus callosum, leads us to think that we are staining oligodendrocytes rather than astrocytes. This glial labeling is not the result of aspecific staining because it was absent from the stained EAAT4$^{-/-}$ sections.

***Cerebellar cortex.*** In the cerebellar cortex, Purkinje cells were intensely immunoreactive, as was the molecular layer. When Triton X-100 was not used for incubating and rinsing the sections (Fig. 3C,D), we could clearly distinguish the dendrites of the Purkinje cells in the molecular layer (Mo). At higher power magnification we could differentiate small dots at the end of the branches of the dendrites, probably representing the dendritic spines (Fig. 3D, arrows), in accordance with the observations of Nagao et al. (1997) and Dehnes et al. (1998). When Triton X-100 was included in the staining protocol, we observed a very dense and homogeneous punctate staining of this layer (data not shown). With neither protocol could we detect EAAT4 labeling in the granular layer (Gr) or the white matter.

***Septal and basal forebrain regions.*** Despite the ubiquitous distribution of EAAT4 protein in the basal forebrain and the septal complex, EAAT4 expression was rather low to moderate, compared with other fore- and

TABLE 1. Distribution of EAAT4 Immunoreactivity in the Rat Brain[1]

| Brain region | EAAT4 Neuropil | EAAT4 Neurons |
|---|---|---|
| Cerebellar cortex | | |
| Purkinje cells | | 2,c |
| Molecular layer | | |
| Granular layer | | |
| Septal and basal forebrain regions | | |
| Lateral septal nucleus | | |
| Medial septal nucleus | | |
| Bed nucleus of the stria terminalis | | |
| Nucleus of the vertical limb of the diagonal band | | |
| Nucleus of the horizontal limb of the diagonal band | | |
| Substantia innominata | | 3 |
| Septohippocampal nucleus | | |
| Septofimbral nucleus | | |
| Septohypothalamic nucleus | | |
| Triangular septal nucleus | | |
| Subfornical organ | | |
| Cerebral cortex | | |
| Isocortex | | |
| Layer I | | |
| Layer II/III | | |
| Layer IV | | |
| Layer V | | |
| Layer VI | | |
| Allocortex | | |
| Piriform | | |
| Cingulate | | |
| Insular | | |
| Perirhinal | | |
| Retrosplenial | | |
| Entorhinal | | |
| Hippocampal formation | | |
| Subiculum | | |
| CA1-3 | | |
| Pyramidal cell layer | | 3 |
| Stratum oriens | | 3 |
| Stratum radiatum | | 3 |
| Dentate gyrus | | |
| Hilus | | 3 |
| Stratum granulosum | | |
| Stratum moleculare | | |
| Dorsal thalamus and metathalamus | | |
| Posterior thalamic nuclear group | | 3 |
| Anteroventral nucleus | | |
| Anterodorsal nucleus | | |
| Anteromedial nucleus | | |
| Laterodorsal nucleus | | |
| Ventrolateral nucleus | | |
| Ventromedial nucleus | | |
| Ventroposteromedial and -lateral nucleus | | |
| Mediodorsal intermediodorsal nucleus | | |
| Dorsolateral nucleus | | |
| Lateral posterior nucleus | | |
| Mediodorsal nucleus | | |
| Centrolateral nucleus | | |
| Centromedial nucleus | | |
| Paratenial nucleus | | |
| Anterior paraventricular nucleus | | |
| Posterior paraventricular nucleus | | |
| Ventral paraventricular nucleus | | |
| Ventral endopiriform nucleus | | |
| Dorsal endopiriform nucleus | | |
| Reticular nucleus | | 3 |
| Paracentral nucleus | | |
| Gelatinosus nucleus | | |
| Rhomboid nucleus | | |
| Reuniens nucleus | | |
| Parafascicular nucleus | | |
| Posterior intralaminar thalamic nucleus | | |
| Subparafascicular thalamic nucleus | | |
| Suprageniculate thalamic nucleus | | 3 |
| Ventral medial geniculate nucleus | | |
| Dorsal medial geniculate nucleus | | |
| Medial medial geniculate nucleus | | |
| Dorsal lateral geniculate nucleus | | |
| Ventral lateral geniculate nucleus | | |
| Epithalamus | | |
| Medial habenula | | |
| Lateral habenula | | |

TABLE 1. (Continued)

| Brain region | EAAT4 Neuropil | EAAT4 Neurons |
|---|---|---|
| Hypothalamus and preoptic region | | |
| Preoptic area | | |
| Suprioptic nucleus | | |
| Anteroventral preoptic nucleus | | 3 |
| Magnocellular preoptic nucleus | | |
| Anterior hypothalamic area | | |
| Lateral hypothalamic area | | |
| Paraventricular hypothalamic area | | |
| Dorsal hypothalamic area | | |
| Ventromedial nucleus | | |
| Dorsomedial nucleus | | |
| Dorsal hypothalamic nucleus | | 2 |
| Periventricular nucleus | | |
| Tuber cinereum area | | 2 |
| Medial tubercle nucleus | | 2 |
| Arcuate nucleus | | |
| Perifornical nucleus | | |
| Periventricular hypothalamic nucleus | | |
| Zona incerta | | |
| Subincertal nucleus | | |
| Amygdaloid complex | | |
| Cortical nucleus | | |
| Amygdalapiriform transition | | |
| Amygdalahippocampal nucleus | | |
| Anterior amygdaloid area | | |
| Anterior cortical nucleus | | |
| Central nucleus | | |
| Basomedial nucleus | | |
| Basolateral nucleus | | |
| Lateral nucleus | | |
| Medial nucleus | | |
| Intercalated nuclei amygdala | | |
| Basal ganglia, ventral thalamus and associated nuclei | | |
| Nucleus accumbens shell | | |
| Nucleus accumbens core | | |
| Striatum (caudate-putamen) | | |
| Globus pallidus | | |
| Subthalamic nucleus | | 3 |
| Substantia nigra pars compacta | | 2,3 |
| Substantia nigra pars reticulata | | 3,4 |
| Substantia nigra pars lateral | | 3,c |
| Entopeduncular nucleus | | |
| Fundus striate | | |
| Ventral pallidum | | |
| Ventral tegmental area | | 2,c |
| Mesencephalic regions | | |
| Interpeduncular nucleus | | |
| Rostral subnucleus | | |
| Caudal subnucleus | | |
| Rostrolateral subnucleus | | |
| Dorsomedial subnucleus | | |
| Apical subnucleus | | |
| Peripeduncular nucleus | | |
| Anterior pretectal nucleus | | |
| Posterior pretectal nucleus | | |
| Nucleus optic tract | | |
| Deep mesencephalic nucleus | | 3 |
| Red nucleus | | |
| Paranigral nucleus | | 2,c |
| Central gray | | |
| Superior colliculus | | |
| Zonal layer | | |
| Superficial gray layer | | |
| Optic nerve layer | | 3 |
| Intermediate gray layer | | |
| Intermediate white layer | | |
| Oculomotor nucleus | | 3 |
| Interfascicular nucleus | | |
| Rostral linear nucleus raphe | | |
| Caudal linear nucleus raphe | | 2,3 |
| Lateral terminal nucleus accessory optic tract | | |
| Prerubral field | | |
| White matter | Glia | |
| Fasciculus retroflexus | | |
| Corpus callosum | | |
| Anterior commissure | | |
| Fornix | | |
| Fimbria hippocampus | | |
| Internal capsule | | |
| Optic tract | | |
| Mammillothalamic tract | | |
| Stria medularis thal | | |
| Commissure superior colliculus | | |
| Cerebral peduncle | | |
| Brachium superior colliculus | | |
| Ventral hippocampal commissure | | |

[1]Relative intensities of neuropil staining and relative number of labeled neurons. low labeling; moderate labeling; high labeling; no labeling.
[2]Very intensely stained neurons.
[3]Solitary, intensely stained neurons with immunopositive dendrites, intermingled with a larger number of faintly stained cell bodies.

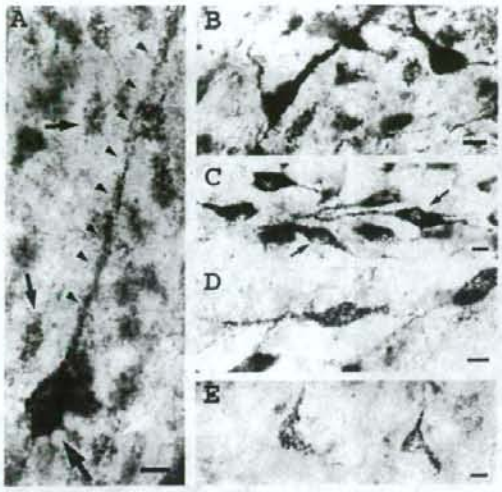


Fig. 2. Detail of EAAT4-immunoreactive neurons in the cerebral cortex (A), VTA (B,C), SNc (D), and prerubral field (E) after staining in the presence of Triton X-100. **A:** Pyramidal neurons of layer V of the cerebral cortex are intensely and homogeneously stained (large arrows). Dendrites of these neurons are visualized as an alignment of immunoreactive puncta (arrowheads). Intermingled with the intensely stained pyramidal neurons, faintly stained neurons could be seen that are composed of labeled granules (small arrows). Also neuropil staining consists of EAAT4-positive granules. **B–D:** EAAT4-IR in the VTA (B,C) and SNc (D). Besides very intensely and homogeneously stained neurons (B, arrow), we could detect neurons with nuclei devoid of this homogeneous and intense IR, although covered with immunoreactive puncta (C, arrows). Some of the neurons, as well as their dendrites, are defined only by these immunoreactive puncta (D). **E:** Two faintly stained neurons located in the prerubral field show a punctate labeling. Scale bar 10 μm in A–E.

midbrain regions (Table 1). We observed relatively strong labeling in the subfornical organ (SFO) (data not shown).

***Cerebral cortex.*** EAAT4-immunoreactive neurons were detected in layers II–VI throughout all subdivisions of the cerebral cortex, the isocortex, and the allocortex (Fig. 3A,B). In general, the strongest labeling was observed in the tightly packed cells of layers II/III as well as in the sparsely distributed, large multipolar pyramidal neurons of layer V (Figs. 2A, 3A,B). Apical dendrites of the pyramidal neurons of layer V could be followed into layer II (Figs. 2A, 3A,B). With the Triton-free staining protocol, IR could be detected predominantly in the somatodendritic compartment of neurons of layers II/III and layer V (Fig. 3A). In Triton-exposed material, cells were abundantly present in all layers of the cerebral cortex, except for layer I (Fig. 3B). The pyramidal cells of layer V are still more intensely stained and the lamination pattern still emerges because of the stronger neuropil staining in layers II/III and V compared with the other layers.

***Hippocampal formation.*** Figure 4 illustrates how IR was readily apparent in the subiculum (S), in principal and nonprincipal cells of the CA1–3 fields of Ammon's horn (hippocampus proper or cornu Ammonis), in the stratum granulosum (sg) of the dentate gyrus (DG), and in scattered larger cells with neuronal morphology in the hilus (H). Because axonal fibers and synaptic terminals were not stained, it was impossible to categorize EAAT4-positive interneurons in terms of the locations of their axonal projections.

On the whole, in the hippocampal formation we observed a punctate or granular, yet very dense and intense, staining of the cell somata (Fig. 4H–J).

In the subiculum (S; Fig. 4A,B), EAAT4-immunoreactive neurons in the pyramidal cell layer (pyr) were plentiful and intensely stained. Dendrites of all neurons could be followed into the molecular layer, where they formed a dense meshwork.

In the dentate gyrus (Fig. 4C), EAAT4-positive neurons were abundantly present in the stratum granulosum (sg) whereas significant numbers of large multipolar cells could be observed in the hilus (H) and a few cells in the stratum moleculare (sm). Although it is a simple matter to identify most hippocampal principal cells anatomically, the principal cells of the dentate hilus (i.e., the glutamatergic mossy cells; Soriano and Frotscher, 1994; Wenzel et al., 1997) are intermingled with hilar interneurons (Amaral, 1978) and therefore cannot be differentiated by using standard staining methods. Nevertheless, neurons within the hilar region showed an intense punctate labeling in addition to the faint homogeneous staining of the cell body (Fig. 4D).

Within CA1–3, EAAT4 expression was observed in the somata and initial part of the apical dendrites of pyramidal cells (Fig. 4E–J). Labeling of the dendrites was manifested as an alignment of a large number of immunopositive puncta (Fig. 4H). Immunoreactive neurons were more densely packed in a more orderly fashion in the stratum pyramidale (sp) of CA1 (Fig. 4E,H) compared with CA2 and CA3 (Fig. 4F,G, I, J). Scattered multipolar neurons were found in the stratum oriens (so) and stratum radiatum (sr).

***Dorsal thalamus, metathalamus, and epithalamus.*** On the whole, EAAT4 expression within the thalamic nuclei was moderate relative to the general staining intensity in the fore- and midbrain, with a few exceptions as described below. Very high expression levels could be detected in the MHb (Fig. 5A). When the remaining regions of the forebrain were still immunonegative, staining of the MHb was already intense, as well as staining of the IP (Fig. 5E,F) and the axon bundle connecting both nuclei, namely, the fasciculus retroflexus (fr; Fig. 5B–E). For the MHb we detected a predominant neuropil staining. In the lateral habenular nucleus (LHb) neuropil staining was significantly lower. However, in this nucleus immunoreactive neurons were abundantly present, contrary to the MHb (Fig. 5A, Table 1). A very intense neuropil staining could be observed in the caudal (IPC) and rostrolateral subnucleus (IPRL) of the IP, whereas staining of the rostral (IPR), dorsomedial, and apical subnuclei was rather moderate (Fig. 5F, Table 1). In frontal (Fig. 5A,B) as well as sagittal (Fig. 5D,E) sections, the striate immunoreactive signal of the fasciculus retroflexus could be traced from the departure of the axon bundle in the habenular nuclei (Hb) until arrival in the IP. On the course from the Hb to the IP, branching of the fibers was observed only once (Fig. 5B, arrows).

***Hypothalamus and preoptic region.*** In general, relatively high expression levels of EAAT4 protein could be observed within the hypothalamic region (Table 1). The different nuclei that compose the hypothalamus could be

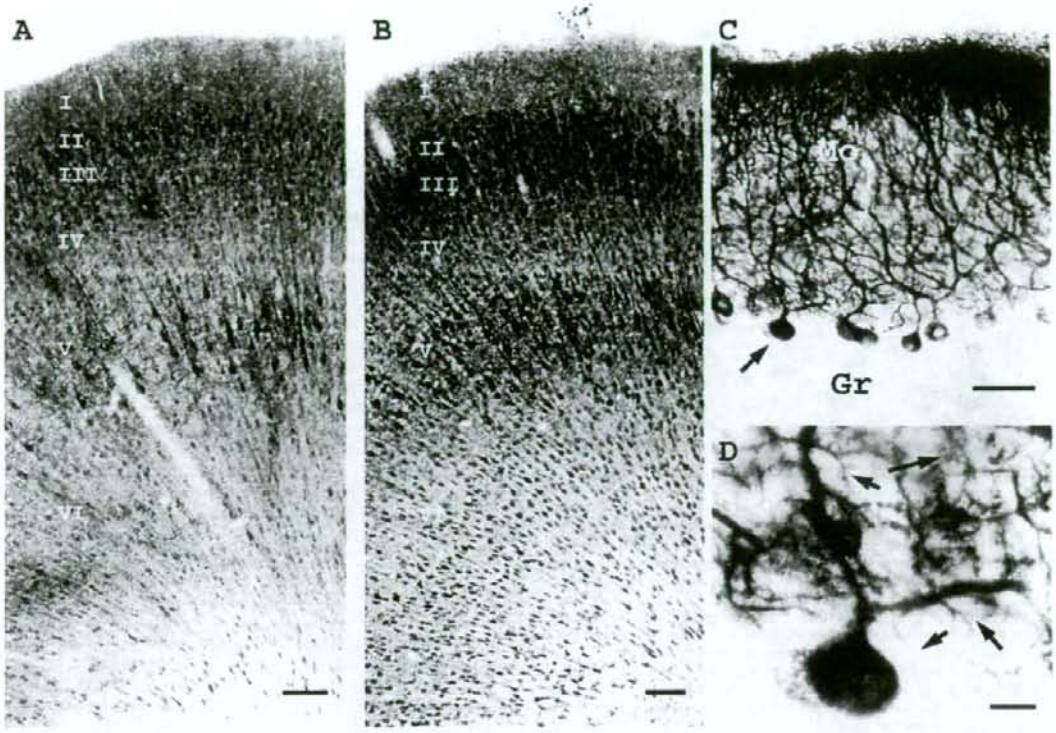


Fig. 3. EAAT4-IR in cerebral (A,B) and cerebellar (C,D) cortex using the EAAT4 antiserum in the presence (B) or absence (A,C,D) of Triton X-100. **A,B:** Immunopositive neurons could be detected in all layers of the cerebral cortex. When Triton was used (B) in the staining protocol, the number of immunopositive cells was significantly higher compared with Triton-free stainings (A). Apical dendrites of the pyramidal neurons in layer V could be followed into layer II. **C:** EAAT4 labeling was highly enriched in the Purkinje cells (arrow) and in the molecular layer (Mo). The granular layer (Gr) was devoid of IR. **D:** Detail of an immunostained Purkinje cell and dendrites in the Mo. Small dots at the ends of the branches are suggestive of dendritic spines (arrows). Scale bar 100 μm in A,B; 50 μm in C; 10 μm in D.

distinguished very easily after staining. Within each nucleus, EAAT4-immunoreactive cell bodies were homogeneously distributed. Except for the dorsal hypothalamic nucleus, in which large intensely immunoreactive multipolar neurons were sparsely distributed and in which immunoreactivity expanded into the dendrites, immunostained cell bodies were rather small and densely packed. Here too, the majority of the cell bodies consisted of a collection of immunoreactive puncta or granules (data not shown).

***Amygdaloid complex.*** In the majority of the nuclei constituting the amygdala, a moderate to relatively high expression level of EAAT4 protein could be observed (Table 1).

***Basal ganglia and associated nuclei.*** EAAT4-positive neurons could be detected in all structures of the

Fig. 4. Expression profile of EAAT4 throughout the hippocampal formation, as visualized by using the staining protocol including Triton X-100. **A:** Overview of EAAT4–IR in a frontal section at Bregma −5.2. **B:** Relatively high expression levels of EAAT4 could be detected in neurons located in the pyramidal layer (pyr) of the subiculum (S). Immunoreactive apical dendrites of the pyramidal neurons expanded into the molecular layer (ml). **C:** Neurons of the stratum granulosum (sg) of the dentate gyrus (DG) were quite intensely stained, as were scattered neurons in the hilus (H). **D:** A higher power photomicrograph of labeled neurons in the hilar region demonstrates the granular staining. **E–J:** Also, the principal cells in the stratum pyramidale (sp) of CA1 (E,H), CA2 (F,I), and CA3 (G,J) show a dense granular EAAT4 labeling (arrows), extending into the initial part of the apical dendrites (H, arrowheads), as well as sparse nonprincipal cells in stratum oriens (so) and stratum radiatum (sr). Abbreviations, Ctx, cerebral cortex; Ent, entorhinal cortex; fr fasciculus retroflexus; LPMC, mediocaudal lateral posterior thalamic nucleus; LT, lateral terminal nucleus accessory optic tract; MG, medial geniculate nucleus; pol, polymorphic layer; SC, superior colliculus; sm, stratum moleculare; SNc, substantia nigra pars compacta; SNr, substantia nigra pars reticulate; VTA, ventral tegmental area. Scale bar 500 μm in A; 100 μm in B,C; 50 μm in E–G; 25 μm in D; 10 μm in H–J

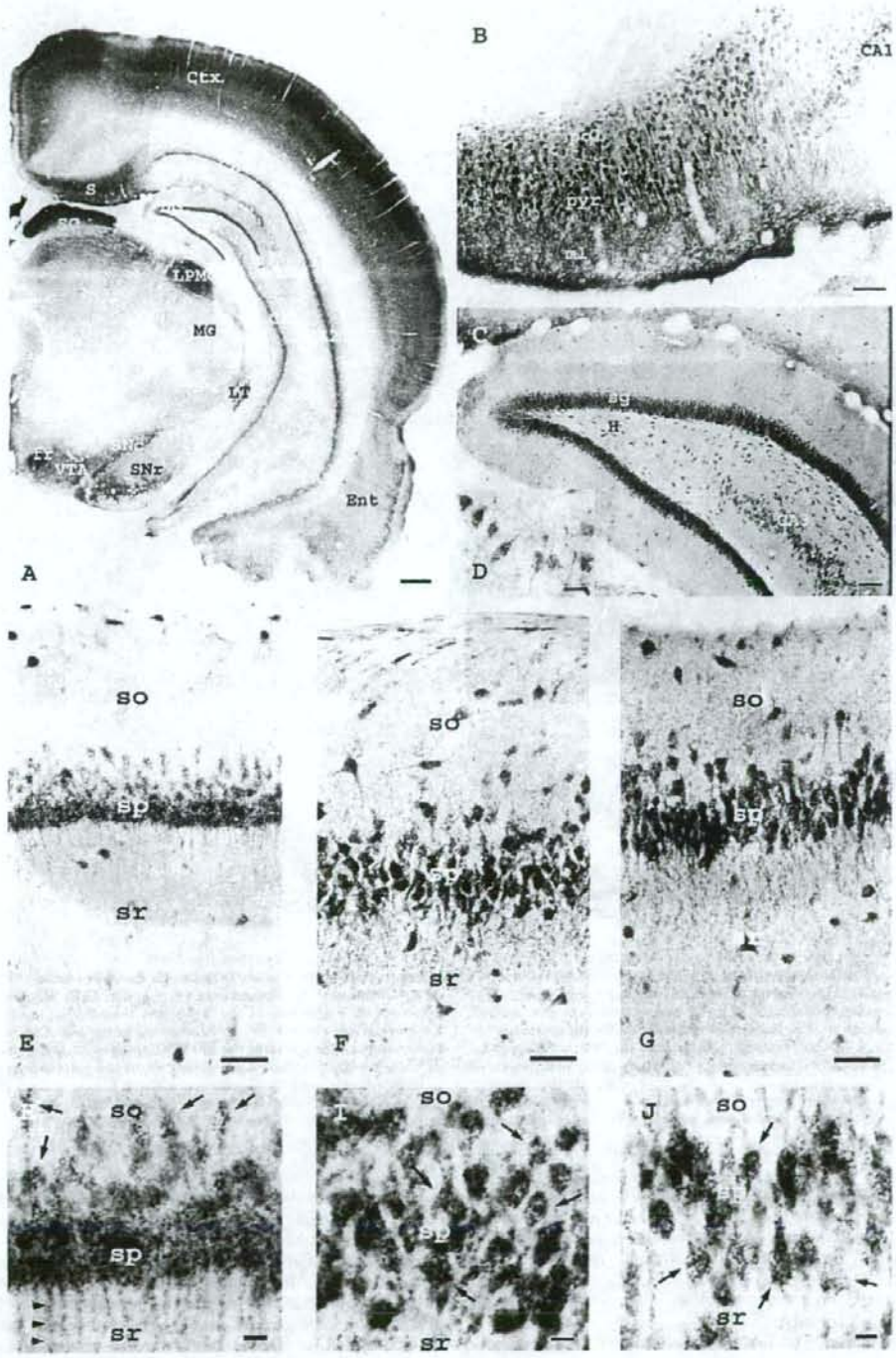


Figure 4

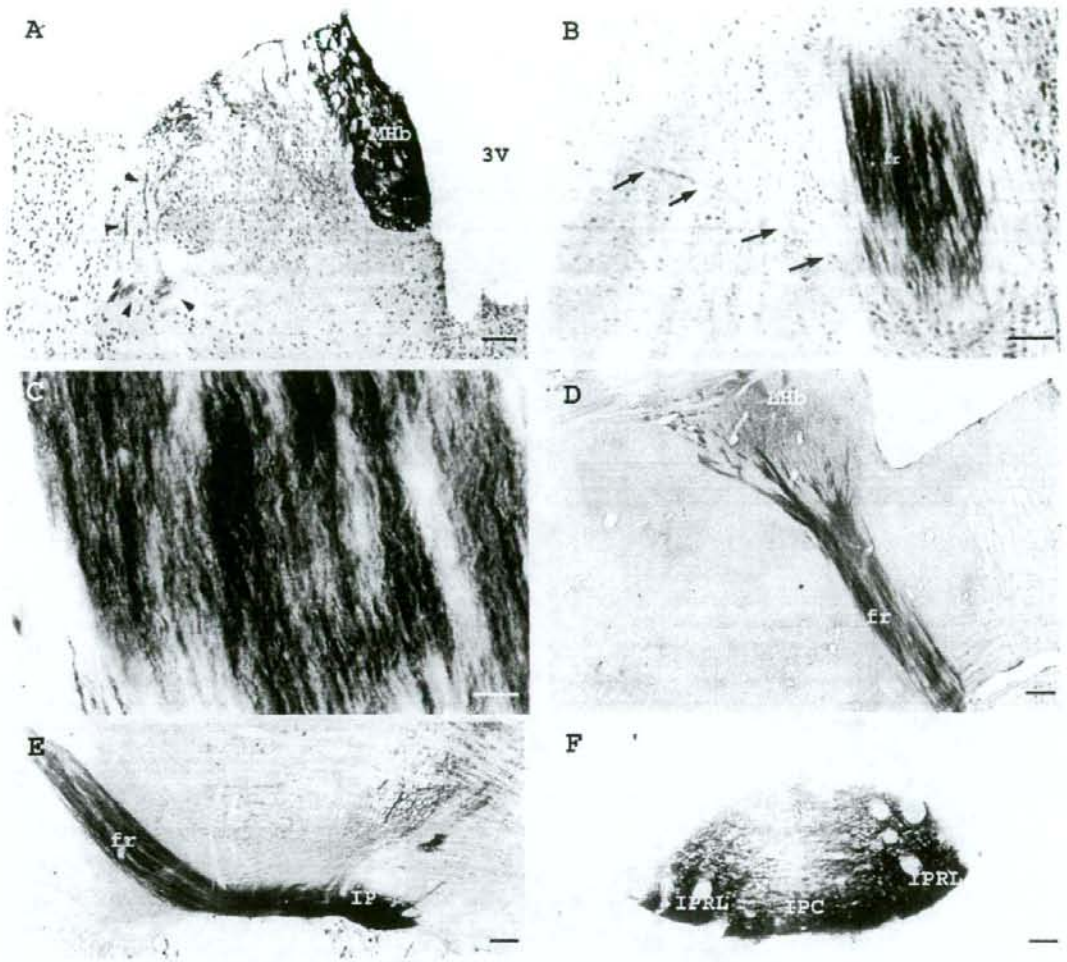


Fig. 5. EAAT4-IR in the presence of Triton X-100, in frontal (A–C,F) and sagittal (D,E) sections through the habenular nuclei (Hb; A,D), the fasciculus retroflexus (fr; B–E), and interpeduncular nucleus (IP; E,F). **A:** In the medial habenular nucleus (MHb) immunoreactivity was confined to the neuropil, whereas in the lateral habenular nucleus (LHb) EAAT4 labeling could be observed in neuronal cell bodies. Arrowheads point to fibers of the fasciculus retroflexus, originating in the habenular nuclei. **B:** An intense striate-like labeling in the fasciculus retroflexus can be seen. Arrows point to an immunoreactive branch of the main bundle. **C:** In more detail, this striate labeling consists of immunoreactive punctae. **D,E:** Sagittal sections demonstrate the course of the fasciculus retroflexus, starting in the Hb and arriving in the IP. **F:** Intense staining was also seen in the rostrolateral subnucleus of the IP (IPRL) and caudal nucleus of the IP (IPC), whereas staining was less intense in the rostral nucleus of the IP (IPR). Abbreviations: 3V, third ventricle; LHbL, lateral part of the lateral Hb; LHbM, medial part of the lateral Hb. Scale bar 100 μm in A,F; 50 μm in B; 25 μm in C; 200 μm in D,E.

basal ganglia, i.e., the striatum (Fig. 6A), globus pallidus (Fig. 6B), subthalamic nucleus (STN; Fig. 6C), substantia nigra (SN; Fig. 6D), and entopeduncular nucleus (EP; Fig. 6E), with the most intensely stained neurons being present in the SNc (Figs. 4A, 6D). In the VTA, a basal ganglia-related structure, labeling was as intense as in the SNc (Figs. 4A, 6F).

In the striatum (Fig. 6A), immunoreactive intermediate-sized neurons were abundantly present, indicating that EAAT4 is present in most of the γ-aminobutyric acid (GABA)ergic efferent spiny neurons that account for 96% of the total neuronal population of the striatum (Ribak et al., 1979; Kita and Kitai, 1988). These immunoreactive cells are homogeneously distributed without any correspondence with patches (striosomes)/matrix compartments (Gerfen, 1992; Hiroi, 1995). EAAT4 labeling was observed exclusively in cell bodies, dendrites being devoid of any staining. In between these intermediate-sized neurons, a few solitary,